In vivo Imaging of Retinal Ganglion Cells and Microglia

LI, Zhiwei

A Thesis Submitted in Partial Fulfilment

of the Requirements for the Degree of

Doctor of Philosophy

in

Ophthalmology and Visual Sciences

The Chinese University of Hong Kong

September 2010

Thesis/Assessment Committee

Professor Vincent Yau Wing LEE (Chair)

Professor Christopher Kai Shun LEUNG (Thesis Supervisor)

Professor Wing Ho YUNG (Committee Member)

Professor Calvin Chi Pui PANG (Committee Member)

Professor Ming Liang PU (External Examiner)

Abstract

Progressive neuronal cell death and microglial activation are the key pathological features in most neurodegenerative diseases. While investigating the longitudinal profiles of neuronal degeneration and microglial activation is pertinent to understanding disease mechanism and developing treatment, analyzing progressive changes has been obfuscated by the lack of a non-invasive approach that allows long term, serial monitoring of individual neuronal and microglial cells. Because of the clear optical media in the eye, direct visualization of the retinal ganglion cells (RGCs) and microglia is possible with high resolution *in vivo* imaging technique. In this study, we developed experimental models to visualize and characterize the cellular morphology of RGCs and retinal microglia *in vivo* in the Thy-1 YFP and the CX3CR1$^{+/GFP}$ transgenic mice, described the patterns of axonal and dendritic shrinkage of RGCs, discerned the dynamic profile of microglial activation and investigated the relationship between RGC survival and microglial activation after optic nerve crush and retinal ischemic injury induced by acute elevation of intraocular pressure.

A confocal scanning laser ophthalmoscope (CSLO) was used to image the axonal and dendritic aborizations of RGCs in the Thy-1 YFP mice. With quantitative analysis of cell body area, axon diameter, dendritic field, number of terminal branches, total dendritic branch length, branching complexity, symmetry and distance from the optic disc, the morphologies of RGCs and the patterns of axonal and dendritic degeneration were analyzed. After optic nerve crush, RGC damage was observed prospectively to begin with progressive dendritic shrinkage, followed by loss of the axon and the cell body. Similar pattern of RGC degeneration was observed after 90 minutes of retinal ischemia although no morphological changes were detected when the duration of ischemia was shortened to 30 minutes. The rate

of dendritic shrinkage was variable and estimated on average 2.0% per day and 11.7% per day with linear mixed modeling, after optic nerve crush and retinal ischemic injury, respectively. RGCs with a larger dendritic field had a slower rate of dendritic shrinkage.

The longitudinal profile of microglial activation was investigated by imaging the $CX3CR1^{GFP/+}$ transgenic mice with the CSLO. Activation of retinal microglia was characterized with an increase in cell number reaching a peak at a week after optic nerve crush and retinal ischemic injury, which was followed by a gradual decline falling near to the baseline at the 4^{th} week. The activation of retinal microglia was proportional to the severity of injury. The number of RGCs survival at 4 weeks post-injury was significantly associated with the number of activated retinal microglia.

In summary, we demonstrated that dendritic shrinkage could be evident even before axonal degeneration after optic nerve crush and retinal ischemic injury. We have established a methodology for *in vivo* and direct visualization of RGCs and retinal microglia, which could provide reliable and early markers for neuronal damage. Measuring the rate of dendritic shrinkage and tracking the longitudinal activation of microglia would provide new paradigms to study the mechanism of neurodegenerative diseases and offer new insights in testing novel therapies for neuroprotection.

摘要

進行性的神經細胞退行病變和巨噬細胞的激活是大多數神經病變的關鍵病理變化。長期以來，對神經細胞壞死和巨噬細胞激活的活體追蹤研究一直受阻於沒有理想的無創傷性的研究技術。眼睛由於其特殊的光學結構，為我們提供了壹個直接觀察視網膜節細胞和巨噬細胞的平臺。在本研究中，我們使用轉基因小鼠建立了直接觀察節細胞和巨噬細胞細胞形態的平臺，定量描述了視網膜神經節細胞樹突和軸突的病理變化，觀察了在視神經擠壓傷和視網膜缺血再灌註傷後巨噬細胞的激活，並探討了其和視網膜神經節細胞存活的關系。

本研究應用共焦激光掃描檢眼鏡觀察 THY-1-YFP 轉基因小鼠的樹突及軸突形態。通過對胞體面積，軸突直徑，樹突面積，樹突終末分支數量，樹突總長度，對稱性，胞體和視盤的距離的記錄，對節細胞形態和樹突軸突的病變模式進行了分析。在視神經擠壓傷模型中，樹突最先壞死，其次為軸突和胞體。同樣的病變模式在受到 90 分鐘缺血損傷的視網膜中發現。沒有在 30 分鐘缺血損傷後觀察到神經節細胞的形態學改變。樹突收縮速率的變異較大，在擠壓傷模型和缺血損傷模型中分別為 2.0% 每天和 11.7% 每天。樹突野面積和收縮速率呈負相關。

本研究應用共焦激光掃描檢眼鏡觀察 $CX3CR1^{GFP/+}$ 轉基因小鼠的巨噬細胞激活模式。視網膜巨噬細胞的數量在視神經擠壓傷和缺血損傷後一周到達高峰，然後以較慢的速率下降，在四周後下降到接近基線的水平。巨噬細胞的激活水平和損傷程度呈正相關。損傷後四到十二周的節細胞數量和巨噬細胞激活程度呈負相關。

綜上所述，本研究表明樹突的收縮在視神經擠壓傷和視網膜缺血損傷後先於

軸突壞死出現。在本研究中我們建立了可以活體直接觀察視網膜神經節細胞和巨噬細胞的平臺。通過此平臺我們可以可靠地檢測到早期神經細胞病變。對樹突收縮的速率和巨噬細胞的激活水平的測量為我們研究神經退行病變的機制和神經修復的方法提供了新的信息。

Acknowledgements

I am most grateful to Associate Professor Christopher K. S. Leung and Professor Calvin C. P. Pang for their valuable advice and guidance. I thank Professor Leung for his inspiring supervision and leading me into the fascinating world of *in vivo* imaging. I thank Professor Pang for his training on my writing and presentation skills, as well as his unceasing support.

I am indebted to Dr. Liu Shu, Dr. Ye Cong and Dr. Liu Lan for their contribution in taking excellent care to the transgenic mice investigated in the study. This work cannot be achieved without their support. Dr. Nathon Choi contributed to designing the programs for morphological parameter analysis.

I would like to thank Assistant Professor Gary H. F. Yam for his insightful comments. I am indebted to Ms. Pancy O. S. Tam and Ms. Winnie W. Y. Lee for their technical assistances in immunohistochemical and genetic analysis.

Part of the study was done in School of Biomedical Science of the Chinese University of Hong Kong, Department of Anatomy of University of Hong Kong, and Department of Anatomy and Embryology of Peking University. I would also like to thank Professor Wing Ho Yung, Kwok Fai So, Ming Liang Pu, and Dr. Qiao Ling Cui for their supports in this study.

Table of Contents

List of Figures

Abbreviations

BBB	blood brain barrier
BDNF	brain-derived neurotrophic factor
BRB	blood retinabarrier
BSA	bovine serum albumin
CFP	cyan fluorescent protein
CLSM	confocal laser scanning microscope
CNS	central nerve system
CR3	complement receptor 3
CSLO	confocal scanning laser ophthalmoscope
CX3CR1	CX3C chemokine receptor 1
DB	die back
ERG	electroretinogram
FBS	fetal bovine serum
GCL	ganglion cell layer
GDNF	glial cell-derived neurotrophic factor
GFP	green fluorescent protein
HRA	heidelberg retina angiograph
ICAM-1	inter-cellular adhesion molecule 1
IL-6	interleukin 6
IOP	intra-ocluar pressure
LFA-1	lymphocyte function-associated antigen 1
Mac-1	macrophage-1 antigen
NGS	normal goat serum
NMDA	N-methyl-D-aspartate
OPL	outer plexiform layer
ONL	outer nuclear layer
PDGF	platelet-derived growth factor
RGC	retinal ganglion cell
RPE	retinal pigment epithelium
RNFL	retinal nerve fiber layer
SLO	scanning laser ophthalmoscope
TNF-a	tumor necrosis factor-alpha

WD	Wallerian degeneration
YFP	yellow fluorescent protein

Publications

Publications based on the work of this thesis

Li ZW, Liu S,Robert N Weinreb, James D Lindsey, Liu L, Ye C, Yung WH, Pang CP, Lam SC, Leung CK. Tracking Retinal Microglia Activation in Relation to Retinal Ganglion Cell Degeneration (Pending submission to *Archives of Ophthalmology*).

Li ZW, Liu S,Robert N Weinreb, James D Lindsey, Liu L, Ye C, Yung WH, Pang CP, Lam SC, Leung CK. Tracking dendritic shrinkage of retinal ganglion cells in retinal ischemia (Under consideration in *Archives of Ophthalmology*).

Leung CK, Robert N Weinreb, **Li ZW**, Shu Liu, James D Lindsey, Nathan Choi, Liu L, Cheung YL, Ye C, Qiu KL, Chen LJ, Yung WH, Jonathan G Crowston, Pu ML, So KF, Pang CP, Lam SC. Long-term *in vivo* imaging and measurement of dendritic shrinkage of retinal ganglion cells (Under consideration in *Investigative Ophthalmology and Visual Science*).

Publications related to the work of this thesis

YinY, Cui Q, Gilbert H. Y. , Yang Y, Yang Z, Berlinicke, C., **Li, ZW**, Zaverucha-do-Valle C., He H, Petkova V., Zack, D. J., Benowitz, L. I. (2009).Oncomodulin links inflammation to optic nerve regeneration. Proc Natl Acad Sci U S A 106(46): 19587-92.

Huang, Y, **Li ZW**, van Rooijen, N, Wang NL, Pang CP Cui Q. (2007). Different responses of macrophages in retinal ganglion cell survival after acute ocular hypertension in rats with different autoimmune backgrounds. Exp Eye Res 85(5): 659-66.

Huang Y, **Li ZW**, van Rooijen, N, Wang NL, Cui Q (2008). Roles of PI3K and JAK pathways in viability of retinal ganglion cells after acute elevation of intraocular pressure in rats with different autoimmune backgrounds.BMC Neurosci 9: 78.

Conference presentations

Li ZW, Yin Y, van Rooijen, N, Benowitz, L. I. , Cui Q (May 2009). Macrophages and

oncomodulin mediate the effects of lens injury in stimulating axon regeneration through a peripheral nerve graft. Association for Rsesearch in Vision and Ophthalmology (ARVO) Annual Meeting.

Li ZW, Cui Q (June 2008Authors list). The gene therapy for age related macular degeneration. World Ophthalmology Congress (WOC).

Li ZW, Liu S,Robert N Weinreb, James D Lindsey, Liu L, Ye C, Yung WH, Pang CP, Lam SC, Leung CK. The dendritic shrinkage of retinal ganglion cells after ischemia reperfusion injury. Chinese Congress of Research in Vision and Ophthalmology (CCRVO) Annual Meeting. Febuary 2010.

Chapter One

Literature Review

1.1 The retinal ganglion cells and the retinal microglia

1.1.1 The anatomy and classification of retinal ganglion cells

Retinal ganglion cells (RGCs) are neurons residing in the inner retina. The cell bodies and the axons constitute the ganglion cell layer and retinal nerve fiber layer, respectively. The RGCs have extensive connection with two types of intermediate neuron: bipolar cells and amacrine cells. The total number of RGCs in human retina is approximately 1.6 million and they receive signals from approximately 125 million photoreceptors (Callaway, 2005). While the RGCs vary in the size of dendritic field, dendritic complexity, and connections with neighboring cells, most of their axons synapse at the lateral geniculate nucleus via the optic nerve, optic chiasm, and the optic tract. The axons of RGCs also synapse in a retinotopic fashion in the midbrain and in the hypothalamus (Pickard, 1982).

RGCs have been categorized into different subsets in mammalian retinas including monkey (Rodieck and Watanabe, 1993; Dacey et al., 2003; Lee et al., 2005), rabbit (Amthor et al., 1983; Rockhill et al., 2002), cat (Boycott and Wassle, 1974; Stone and Clarke, 1980; Isayama et al., 2000), rat (Perry, 1979; Sun et al., 2002b)and mouse (Doi et al., 1995; Kong et al., 2005). RGCs can be classified according to the morphology (Dacey et al., 2003; Kong et al., 2005), immunology (Coombs et al., 2006), function and projection pattern (Martin, 1986).

With immunochemical staining, intracellular injection labeling, or transgenic fluorescent protein expression, detailed cellular morphology of RGCs can be identified. At least 26 morphological parameters have been used to classfy RGC subsets, These parameters include: 1) dendritic field area, 2) Mean stratification depth of dendritic arbor in IPL, 3) Standard deviation of dendritic arbor stratification depth in the IPL, 4) Distance in

microns from cell body to mean dendritic arbor stratification along z-axis,5) Asymmetry value, 6) Number of branch points within dendritic arbor, 7) Number of branch points/ dendritic field area, 8) Total dendritic length/ dendritic field area, 9) Total terminal dendritic segment length/ dendritic field area, 10) Total nodal dendritic segment length/ dendritic field area, 11) Total dendritic length, 12) Mean dendritic segment length, 13) Total terminal dendritic segment length 14) Mean terminal dendritic segment length 15) Total nodal dendritic segment length 16) Mean nodal dendritic segment length 17) Total terminal dendritic segment length/total nodal dendritic segment length, 18) Mean terminal dendritic segment length/mean nodal dendritic segment length, 19) Segment tortuosity mean, 20) Segment tortuosity standard deviation, 21) Nodal tortuosity mean, 22) Nodal tortuosity standard deviation, 23) Planar angle mean, 24) Planar angle standard deviation, 25) Local spline angle mean, and 26) Local spline angle standard deviation (Kong et al., 2005; Coombs et al., 2006). More than 11 subsets of RGCs have been identified in mouse retina (Badea and Nathans, 2004; Kong et al., 2005; Coombs et al., 2006). The identity of different clusters can be evaluated by morphology (Sun et al., 2002b; Badea and Nathans, 2004; Kong et al., 2005), or in combination with the expression patterns of certain antigens identified by immunohistochemical staining (Coombs et al., 2006). The major subsets are constituted by monostratified cells, in which the dendrites are confined to either on or off the sublaminae of the inner plexiform layer; the other subsets are bistratified cells, in which dendrites are located in the on and off sublaminae.

With reference to the projection pattern and function, five main groups of RGCs can be classified. Midget RGCs project to the parvocellular layers of the lateral geniculate nucleus. Midget cells are responsible for detecting fine details and color vision. Midgetcells constitute about 80% of RGCs (Rodieck et al., 1985; Watanabe and Rodieck, 1989). Parasol RGCs project to the magnocellular layers of the lateral geniculate nucleus. They

have larger cell bodies and dendritic field and are sensitive to visual stimuli that changes quickly over time. Parasol cells participate in the detection of motion (Ji et al., 2005). Parasol cells present sustained action potentials as long as the presence of stimulus. Parasol cells constitute approximately 10% of the RGC population (Rodieck et al., 1985; Watanabe and Rodieck, 1989). Bistratified RGCs project to the koniocellular layers of the lateral geniculate nucleus. They receive inputs from intermediate numbers of rods and cones, and can respond to moderate-contrast stimuli (Malpeli and Baker, 1975; Leventhal et al., 1981; Naito, 1989; Szmajda et al., 2008). Photoreceptive ganglion cells, also called photosensitive RGCs, have a unique role in the visual system. They respond slowly to light stimulus, but are intrinsically photosensitive. Even the electrical stimulus from photoreceptor is blocked, photoreceptive ganglion cells can present action potentials in response to light stimuli. Compared to the rods and cones, the photoreceptive ganglion cells respond to light over a longer term (Wong et al., 2005). Their functional roles are not image forming. They provide a stable representation of ambient light intensity, participate in synchronizing circadian rhythms to the 24-hour light/dark cycle (Berson et al., 2002; Garbarino-Pico et al., 2004), and contribute to photic regulation of melatonin release from the pineal gland (Lucas et al., 1999). A minority of RGCs project to the Edinger-Westphal nucleus (EW) for control of the pupillary light reflex.

1.1.2 The function of retinal ganglion cells

RGCs are the final output neurons in the vertebrate retina. Bipolar cells and amacrine cells provide information to RGCs in the form of chemical messages. These messages are sensed by the receptors on the ganglion cell membrane and transformed into intracellular electrical signals. These signals are integrated and digitized inside RGCs and send out in action potentials. The action potentials transmit information in a time-coded

digital form over long distances through the optic nerve to the brain. Different subtype of RGCs has its unique sensitivity to detect a certain subtle features of the visual scene, including color, size, direction and speed of motion. The main termination of RGC axons is the lateral geniculate nucleus. However, certain subset of RGCs has their specific terminations depending on the information they encode. According to the relation of the initiation of RGC action potential and light stimulation, RGCs can be classified into 3 subtypes (Carcieri et al., 2003). The "ON" type cells respond with a transient burst to light onset, and a sustained elevated discharge rate throughout the light stimulation. The "ON-OFF" type cells respond with discharge bursts to the onset and cessation of light stimuli, but keep quiet during the duration of stimuli. The "OFF" type cells keep quiet until the cessation of light stimuli (Hartline, 1938).

The contrast sensitivity reflects the characteristic 'spatial tuning' of RGC receptive fields. The different contrast sensitivity of objects with different size reflects in part the variable dendritic span in the RGCs The concept of receptive field, introduced by Hartline (Hartline, 1938), reflects the spatial property of RGCs. The RGC receptive fields are fixed in space and immobile, typically do not extend beyond 1 mm in diameter, and are graded in sensitivity over a particular region. The central area of a receptive field is more sensitive to visual stimuli compared with the peripheral part.

RGCs receive color information from cone photoreceptors. In addition, RGCs also transmit a monochromatic, non color containing signal from rods. The peak of spectral sensitivity of rods is about 500nm. Rods can detect a single photon (Hecht et al., 1942; Van Der Velden, 1946). Retinal ganglion cells have no true threshold for detection of dim stimuli. When responses are averaged, signals can be seen for light stimuli as dim as desired, and this includes stimuli that only a few physical quanta of light. Of course in total darkness retinal ganglion cells still exhibit a maintained but variable spontaneous firing rate

and it is against this background noise that quantal responses must be detected.

1.1.3 The anatomy and classification of microglia

Macrophages refer to monocyte derived cells in the tissue. Depending on the tissue location, macrophages may be named differently (Table 1.1). In general, macrophages in the central nervous system (CNS) can be phenotypically classified into four categories: infiltrated macrophages, pericytes, perivascular macrophages, and the resident microglial cells (Guillemin and Brew, 2004) (Figure 1.1). Microglia account for most of the macrophages in the CNS under physiological condition.The origin of microglia is rather controversial. It is believed that they are derived from hematogenous monocytes or directly from mesenchymal progenitor cells in the early stage of development. The precursor cells invade the CNS during the embryonic, fetal, or perinatal stages, and transform from globoid or amoeboid to ramified shape (Perry et al., 1985; Hickey and Kimura, 1988; Barron, 1995). Perivascular macrophages are a population of migratory macrophages (Bechmann et al., 2001). Pericytes are generally regarded as being transformed from mesodermal cells (Thomas, 1999). During the later stages of blood vessels formation during development, mesodermal cells migrate around blood vessels and the mesenchymal precursor cells travel to the newly formed capillary sprouts and differentiate into pericytes and become enclosed within the basal lamina (Rhodin and Fujita, 1989). Microglia exhibit two phenotypes: amoeboid microglia and the ramified microglia. Amoeboid microglia appear transiently in the developing brain. They are also the activated form of microglia during tissue damage and repair. The ramified form is the most common phenotype (Ling and Wong, 1993). They are regarded as the resting microglia.

1.1.4 The distribution and function of microglia in the retina

The distribution of microglia in the retina is species-specific. Microglia in primate retina are located in the OPL, ONL, GCL and RNFL (Vrabec, 1970; Boycott and Hopkins, 1981). In rats, they are located in the GCL and IPL (Kohno et al., 1982). In cats, microglia evenly distribute within all retinal layers (Boycott and Hopkins, 1981). In terms of the spatial distribution, microglia within GCL and IPL distribute evenly from peripapillary region to *orra serrata* region (Thanos, 1992). The microglia distribute in a territorial pattern. Their dendrites do not overlap.

The functions of microglia in normal retina include homeostatic surveillance, detection of pathologic changes, antigen presentation, and phagocytosis. Microglia processes and arborizations are highly mobile under normal conditions (Davalos et al., 2005; Nimmerjahn et al., 2005). The microglia scan the micro-environment without disturbing the neurons and their fine connections. Resting microglia form a network of potential immunoeffector cells. They are considered to play a critical role in host defense against invading microorganisms, immunoregulation, and tissue repair (Chen et al., 2002). It has been shown that some microglial cells have characteristics of dendritic antigen-presenting cells (Provis et al., 1996). Microglial cells, therefore, have the capability of both antigen presentation and phagocytosis.

1.2 The response of retinal ganglion cells to optic nerve or retinal injury

1.2.1 Degeneration of retinal ganglion cells

1.2.1.1 Axonal degeneration

RGCs have a high metabolic rate because of constant antegrade and retrograde transport along the axonal bundles. The increase in energy demand renders RGCs

vulnerable to hypoxic injury, oxidative damage, and mechanical stress secondary to elevation of intraocular pressure (Sparrow et al., 2002). The non-myelinated portion of the axons extending from the retina to the lamina cribrosa (LC) have an "impedance mismatch" (Wang et al., 2003) requiring more energy to maintain physiological functions. Degeneration of RGCs is evident morphologically byas progressive changes in the axons and dendrites.

The axons of RGCs undergo two types of degeneration: Wallerian degeneration (WD) and dying back (DB) (Figure 1.2). WD occurs in response to focal and acute axonal injury, such as transection, ischemia, and other injuries blocking axonal transport. Calcium influx is one of the primary events (Krause et al., 1994), which is followed by an early form of axonal degeneration - acute axonal degeneration (AAD). AAD, rather than axonal retraction, contribute the loss of the proximal ends (Thompson et al., 2006). After departing from the soma, the distal axons disintegrate in an orderly manner. The process involves breakdown of the endoplasmic reticulum, microfilament, microtubule and neurofilament degradation, mitochondrial swelling and lysis, and myelin collapse (Whitmore et al., 2005). Axonal debris is phagocytosed by surrounding glial cells or invading macrophages if the brain blood barrier (BBB) is compromised. WD is characterized by accumulation of 'dense bodies' and 'neuroaxonal spheroids' and the formation of axonal 'retraction balls' (Griffin et al., 1996; Beirowski et al., 2005; Graeber et al., 2002).

Compared with WD, DB is a slow process. The axons degenerate over weeks or months. DB initiates with the withdrawal of synapse and the axon degenerates from the distal end towards the soma. DB shares a similar microscopical feature with WD. DB cannot be distinguished from WD at a single site of the axon (Bouldin and Cavanagh, 1979; Cavanagh, 1979). However, the two process can be diffrenetiated by the type of injury (chronic stress versus acute axonal injury), the speed of degeneration . DB is characterized

by asynchronous centripetal progression (Spencer and Schaumburg, 1977a, b; Graeber et al., 2002). Previous studies have questioned whether WD and DB are related and share a common pathway. Spencer et.al found that WD spread anterogradely (Lubinska, 1977; Spencer and Schaumburg, 1977b, a; George and Griffin, 1994). In the Wld^s transgenic mouse, both WD and DB were observed to be slow (Perry et al., 1990; Glass et al., 1993; Whitmore et al., 2005). It is possible that DB and WD are two extremes of a range of possible stress responses of the axon(Whitmore et al., 2005). It is evident that a milder focal injury causes the distal axon to degenerate retrogradely in a more DB-like manner whereas a more severe focal lesion produces a rapid anterograde breakdown of the axon (Beirowski et al., 2005).

1.2.1.2 Dendritic degeneration

Dendritic shrinkage is an early response to a wide range of progressive neurodegenerative diseases (Fiala et al., 2002) including glaucoma (Morgan, 2002), Huntington's disease and Alzheimer's Disease (Whitmore et al., 2005). Weber demonstrated that structural abnormalities of the dendrites are the earliest marker of pressure induced RGC degeneration (Weber et al., 1998). The early dendritic pathology includes decrease in dendritic thickness, branching complexity and dendritic field. Considering the extensive bioactivities of dendrites, including harbouring synapses and transmiting electrical stimulation within and between neurons, it is conceivable that dendritic degeneration is closely related to functional impairment of RGCs.

1.2.1.3 Synaptic degeneration

Previsous evidence showed that synapses dgenerate through independent,

compartmentalised programmes (Gillingwater et al., 2002). There are a number of possible pathways involved in the degeneration process: synchronous or asynchronous withdrawal of synaptic boutons and fragmentation. None is involved in WD of axons (Gillingwater and Ribchester, 2003). In neurodegenerative diseases, degeneration of synapses has been shown to precede neuronal cell death (Mattson et al., 1998a; Mattson et al., 1998b; Mattson, 1999, 2000; Gillingwater and Ribchester, 2003; Gelbard, 2004).

1.2.2 Molecular mechanisms of retinal ganglion cell degeneration

The molecular mechanisms signaling RGC degeneration remain elusive. After neuronal injury, there is re-distribution and increase in concentration of intra-axonal calcium. This occurs in an early stage and is a critical feature of axonal degeneration. Many of the subsequent molecular events are calcium dependent (Figure 1.3) (Schlaepfer, 1971, 1974; Ouardouz et al., 2003). The opening of sodium channel is triggered by stress-induced depolarization, which in trun results in the opening of calcium channels. The physiological function of sodium-calcium transporter locating on the outer membrane is then interfered (Brown et al., 2001; Nikolaeva et al., 2005; Whitmore et al., 2005). The elevation of intra-axonal calcium concentration causes the activation of IP3 (Avramut and Achim, 2003; Nikolaeva et al., 2005) and ryanodine receptors (Walton et al., 1991; Avramut and Achim, 2003; Stys, 2004), which in turn releases more calcium from the internal stores and further elevates the calcium level. These processes are in a positive feedback pattern. The increased calcium level stimulates numerous calcium dependent proteases including procaspase-12 (Whitmore et al., 2005) and calpain (Kanje et al., 1985; Zalewska et al., 1986; Bernier et al., 1999), which in turn degrades actin microfilaments and neuronfilaments. The microtubules system is then destructed after activation of calcium dependent proteases. The mitochondria absorb large quantity of calcium inside the neurons.

When the calcium level reaches a critical level, the mitochodria triggers the release of cytochrome C (Buki et al., 2000; Buki and Povlishock, 2006). At the same time, calcium interacts with the permeability transition pore complex (Nicholls, 2009), which increases the permeability and causes mitochodria swelling. The rupture of outer membrane leads to release of cytochrome C from the intermembrane space (Nicholls, 2009), which is followed by proteolysis. The loss of mitochondria accelerates cellular degeneration.

1.3 The responses of microglia in retinal ganglion cell degeneration

The inflammatory responses triggered by tissue injury induce dramatic activation of resident microglia and blood derived macrophages (Suzumura et al., 1987; Schroeter and Jander, 2005). Microglia are involved in invasion, migration, phagocytosis of cellular and myelin debris, and secretion of chemokine, cytokine, and neutrophic factors.

After being activated, the microglia migrate and invade into the lesion site by responding to the chemotactic stimuli from degenerating axons, myelin debris, and complement factors (Bruck and Friede, 1991; Hall, 1993; Bruck et al., 1995) through expression of adhesion molecules, including Mac-1 and LFA-1 (Beuche and Friede, 1986), interaction with ICAM-1 expressed on the endothelial cells (Castano et al., 1996).

Microglia participate in clearing up the myelin and axonal debris via the CR3 receptor (Bruck and Friede, 1991; Bruck et al., 1992).The myelin is an axon regeneration inhibitor. The clearance of myelin is important for both axonal degeneration and regeneration. Microglia also synthesize complement components during phagocytosis (Bruck and Friede, 1991).

Microglia secrete IL-6, phospholipase A (Paul and Gregson, 1992), apolipoprotein E (Muller and Minwegen, 1987), lysozyme (Venezie et al., 1995), TNF-a (Stoll et al.,

1993), BDNF (Bomstein et al., 2003; Bouhy et al., 2006), PDGF (Uutela et al., 2004), and GDNF (Batchelor et al., 1999). After phagocytosing cellular debris, microglia present antigens to lymphocytes, thereby activating the antigen-specific arm of the immune response, and participating in the activation of T cells and the extensive downstream inflammatory responses (Suzumura et al., 1987). Since microglia involve in diverse pathways of neuronal degeneration and regeneration, it is difficult to discern the exact contribution of microglia in degenerating neurons.

1.4 *In vivo* imaging of retinal ganglion cells and microglia

In vivo imaging is a relatively new technique to visualize RGCs and microglia. The first demonstration of *in vivo* imaging of RGCs was reported by Sabel et al. in 1997 (Sabel et al., 1997). They used a confocal laser scaning microscope with adjusted optics combined with injection of fluorescent latex beads into the superior colliculus to image the RGCs in rat (Sabel et al., 1997). Using a similar experimental design, Thanos et al imaged the RGCs with a modified conventional epifluorescence microscopy (Thanos et al., 2002)). Cordeiro et al intravitreally injected Alexa Fluor 488-labeled annexin 5 to image apoptosis of retinal cells with a confocal scanning laser ophthalmoscope (CSLO) . Figure 1.4 shows a schematic diagram of an CSLO. With the addition of adaptive optics, Gray showed that it was possible to image the axons and dendritic aborization of RGCs by retrograde-labeling with rhodamine dextran in a primate model (Gray et al., 2008). All these techniques, however, are invasive requiring retrograde labeling or intravitreal staining of RGCs. Leung et al developed a blue-light CSLO to image the RGCs in the Thy-1 CFP mice non-invasively (Leung et al., 2008a; Leung et al., 2009). Thy-1 is a cell-surface glycoprotein expressed by projection neurons in many parts of the nervous system (Morris, 1985). In the retina, it is largely expressed in the RGCs (Barnstable and Drager,

1984). In the Thy-1 CFP mice, over 90% of RGCs are instrinsically labeled with the cyan fluorescent proteins. Blue-light CSLO has been shown reliable to follow changes in RGC density following optic nerve crush (Leung et al., 2008a) and retinal ishemic injury (Leung et al., 2009).

A number of studies have been conducted using a transgenic mice model to image the retinal microglia *in vivo*. Using a confocal scanning laser microscope (CSLM) to image retinal explants of the CX3CR1$^{GFP/+}$ mice, Lee et al demonstrated the extension and retraction movements of the cellular process of microglia . Eter et al. imaged the CX3CR1$^{GFP/+}$ mice with an CSLO after focal argon laser coagulation to the retina (Eter et al., 2008). They showed accumulation of microglia after 1 to 4 days of injury and that the number of accumulated microglial cells was proportional to the size and intensity of laser spot (Eter et al., 2008). Paques et al showed locomotion of individual microglia in the CX3CR1$^{GFP/GFP}$ mice with an CSLO after focal laser damage to the retina (Paques et al., 2006). The key advantage of using an CSLO over an CSLM is the feasibility to perform *in vivo* imaging thereby permitting long term monitoring of cellular changes.

The CSLO was originally developed by Webb and colleagues (Webb et al., 1987). Imaging is performed with a laser beam passing through an aperture which is then focused by an objective lens into the target. Confocal optics ensures any stray, out-of-focus light is suppressed and thus enhancing the image contrast. Compared with conventional opthalmoscope, CSLO can obtain higher-resolution optical images with depth selectivity.

In this study, the Heidelberg retina angiograph 2 (HRA2), a commercially available model of CSLO, was used to image the RGCs and microglia. The 488nm optically pumped semiconductor laser of the HRA2 was used in this study to excite the YFP (excitation wavelength 514nm) and GFP (excitation wavelength 480nm) in the Thy-1 YFP mice and the CX3CR1$^{GFP/+}$ mice, respectively.

Chapter Two

Objectives

The objectives of this research project were to develop two experimental models based on *in vivo* imaging of retinal ganglion cells (RGCs) and microglia to study the longitudinal profiles of RGC degeneration and microglial activation after optic nerve and retinal ischemic injury.

2.1 *In vivo* imaging of dendritic and axonal arborizations

The introduction of a strain of transgenic mice that express fluorescent protein in the RGCs under the control of a neuron-specific fragment of the Thy-1 promoter offers a non-invasive method for long-term monitoring of progressive neuronal changes (Feng et al., 2000). We recently modified a confocal scanning laser ophthalmoscope (CSLO) to image RGCs in a strain of transgenic mice expressing cyan florescent protein under the control of the promoter for Thy-1 (Thy1-CFP23Jrs mice) (Leung et al., 2008b; Leung et al., 2008a; Leung et al., 2009). Although individual RGC bodies can be identified, axon and dendritic arborization cannot be visualized in this animal strain *in vivo*. Another mouse strain that can be used for *in vivo* visualization of RGC is Thy1-YFP16Jrs mice. Because of strain-to-strain variation in transgene expression (Feng et al., 2000), less than 1% of RGCs are labeled. The YFP expressing RGCs likely represent a random sample of the retina as it has been shown that the expression has no predilection for specific subtypes of RGCs (Coombs et al., 2006). The relatively low density of YFP positive RGCs in the retina of these mice facilitates visualization and demarcation of dendritic arborization of individual RGCs as interference from adjacent cells would be minimal. We have developed an imaging model using an CSLO to study axonal and dendritic degeneration in the Thy1-YFP16Jrs transgenic mice. This technique allows long-term *in vivo* examination of dendritic and axonal structures in live animal without even the need of local or systemic anesthesia. With quantitative analysis of a number of somatic, axonal and dendritic parameters, we

characterized the morphology of RGCs, described the patterns of axonal and dendritic degeneration, identify morphological predictors for cell survival, and estimated the rate of dendritic shrinkage after optic nerve crush.

2.2 Longituidnal profiles of retinal ganglion cell degeneration after ischemic injury induced by elevation of IOP

Acute angle closure and retinal vascular occlusion are common forms of retinal ischemic insults encountered in clinical practice. Loss of retinal ganglion cells (RGCs) and impairment of visual function are inevitable with retinal ischemia if the duration of ischemia is prolonged. Understanding the time course of neuronal degeneration following ischemic injury is thus pertinent to identifying a potential window for therapeutic intervention. In experimental investigation, a conventional model to induce retinal ischemia is to increase the intraocular pressure (IOP) above the retinal perfusion pressure (typically above 90mmHg in murine) (Smith GG, 1952; Buchi et al., 1991; Zhu et al., 2002). RGC damage then is examined by counting the RGC number in a retinal whole mount after their retrograde labeling with a neuronal tracer. This approach, however, only allows cross-sectional analysis of RGC survival at a specific time point after the injury. Using a blue-light confocal scanning laser ophthalmoscope (bCSLO) to serially image the Thy-1 CFP mice (a transgenic mice model with retinal neurons intrinsically labeled with cyan fluorescent proteins under the control of the Thy-1 promoter) *in vivo*, we observed variable loss (14.5% - 79.5%) of RGCs after elevating the IOP to 115 mmHg for 90 minutes (Leung et al., 2009). Notably, there was no detectable reduction in the number of RGCs when the duration of ischemia was shortened to 45 minutes. We hypothesized that dendritic shrinkage would be an early sign of RGC dysfunction and might be evident even after a short duration of ischemia. We used an CSLO to image and follow the changes of axonal

and dendritic arborizations of RGCs after a short (30 minutes) and a long (90 minutes) period of ischemia, and measured the respective rate of dendritic shrinkage.

2.3 *In vivo* imaging of microglia after optic nerve crush and retinal ischemic injury

RGC degeneration has been closely linked with microglia activation. However, the limitation in studying microglial activation is the lack of an efficient model to follow retinal microglial. Published data on the longitudinal profile of microglial activation is sparse. The avaibility of the CX3CR1$^{GFP/+}$ transgenic mice has facilitated *in vivo* visualization of retinal microglia (Kezic et al., 2008). CX3CR1 is a chemokine receptor expressed by microglial. By replacing one copy of the fractalkine receptor gene with a copy of the green fluorescent protein (GFP), it is possible to image the florescent microglia *in vivo* with an CSLO. Using laser coagulation on the retina, Eter et al showed that microglial cells migrated and accumulated to the laser spots (Eter et al., 2008). With time-lapse confocal microcopy on retinal explants, Lee et al demonstrated that microglial increased their motility and transform from symmetric to polarize toward the laser spot after focal laser injury . While these studies provide valuable information on the migration pattern of retina microglia after focal injury to the retina, the longitudinal profile of microglia activation and proliferation after optic nerve damage has not been investigated. We imaged the CX3CR1$^{GFP/+}$ transgenic mice with an CSLO and followed the changes of retinal microglia after optic nerve crush and retinal ischemia.

Chapter Three

Materials and Methods

3.1 Materials

3.1.1 Animals

Three to 6-month-old transgenic mice in which Thy-1 promoter sequences drive the expression of the enhanced yellow fluorescent protein (YFP), designated B6.Cg-TgN Thy1-YFP 16Jrs, were generated by Feng and associates (Feng et al., 2000). One to 3-month-old transgenic mice in which green fluorescent protein (GFP) is expressed under the control of CX3CR1 promoter, designated F1 B6xCx3Cr1-GFP, were generated by Jung (Jung et al., 2000). Breeding pairs of the Thy1-YFP16Jrs mice and the B6xCx3Cr1-GFP mice were obtained from the Jackson laboratory (Bar Harbor, ME).

The living environment of experimental animals was kept at 21°C with a 12-hour light and 12-hour dark cycle. All mice were fed with *ad libitum*. Animals used in this study were treated in accordance with the Chinese University of Hong Kong Animal Experimentation Ethic Committee (AEEC) guidelines and were approved by the AEEC. All possible measures were taken to minimize suffering and limit the number of mice used in this study.

3.1.2 Chemicals

Neurofilament H non-phosphorylated (SMI 32) monoclonal antibody (SMI-32R)	Covance company, U.S.A.
Iba1 polyclonal antibody	Abcom company, U.S.A.
Rhodex red-X-conjugated secondary antibody	Jackson ImmunoResearch company, U.S.A.
N-methyl-D-aspartic acid (NMDA)	Sigma-Aldrich company, U.S.A.
Alex fluroa 488 secondary antibody	Invitrogen Molecular Probes company, U.S.A.
Clodronate liposome and PBS liposome	Professor Nico van Rooijen (Vrije Universiteit, Department of Molecular

	Cell Biology), Holand
Xylazine (2%W/V)	Alfasan company, Holand
Ketamine (10% W/V)	Alfasan company, Holand
Paraformaldehyde	Sigma-Aldrich company, U.S.A.
0.9% sodium chloride solution	Baxter company, U.S.A.
Dorminal (20% W/V)	Alfasan company, Holand

3.1.3 Solutions and buffers

Fixative solution (PH=7.4)	4% (W/V) paraformaldehyde in PBS
Primary antibody blocking solution (For RGC immunostaning) (PH=7.4)	10% normal goat serum (NGS), 2% bovine serum albumin (BSA), 0.5% Triton X-100 PBS
Primary antibody blocking solution (For macrophage immunostaning) (PH=7.4)	10% fetal bovine serum (FBS), 0.5% Triton X-100, PBS
Primary antbody solution (For RGC immunostaining) (PH=7.4)	5% normal goat serum (NGS), 1% bovine serum albumin (BSA), 0.3% Triton X-100, PBS
Primary antbody solution (For macrophage immunostaining) (PH=7.4)	5% fetal bovine serum (FBS), 0.5% Triton X-100, PBS
NMDA solution	40mM NDMA, ddH_2O
Anesthetic	ketamine 0.9 mg/ml xylazine 0.13 mg/ml 0.9% sodium chloride solution

3.1.4 Imaging instruments

The Heidelberg retina angiograph (HRA2), a commercially available model of

CSLO, was used to image the RGCs and the microglia. The HRA2 is installed with two laser sources (488 nm and 795 nm, barrier filters at 500 nm and 810 nm) designed to excite fluorescein and indocyanine green designed for retinal and choroidal angiography. Images can be captured at a speed up to 16 frames per second with image size ranges between 384x384 pixels and 1536x1536 pixels. The digital pixel resolution is 5-10μm/pixel. The field of view ranges between 15°× 15° and 55°× 55°. The focus range is between -24 and +40 diopters. The 488nm optically pumped semiconductor laser of the HRA2 was used in this study to excite the YFP (excitation wavelength 514nm) and GFP (excitation wavelength 480nm) in the Thy-1 YFP mice and the $CX3CR1^{GFP/+}$ mice, respectively.

Confocal laser scanning microscope (Nikon C1 Confocoal system, Tokyo, Japan) was used for imaging retinal flatmount.

3.1.5 Softwares

The CSLO images were exported to a computer for image analysis using a program written under MATLAB R2007a (The MathWorks, Inc., Natick, Massachusetts, USA) computing language environment. Statistical analysis was performed with STATA 10.0 (StataCorp., College Station TX) and SPSS (SPSS Inc, Chicago, Ill).

3.2 Methods

3.2.1 In vivo imaging

The 488 nm optically pumped semiconductor laser in the confocal scanning laser ophthalmoscope (CSLO) (HRA2, Heidelberg Engineering, GmbH, Dossenheim, Germany) was used to detect the fluorescent signal in the RGCs and microglia (Figure 3.1). A 55°

wide field lens was added to the camera to increase the field of view of the fundus.The imaging procedure was performed with one technician gently holding the animal and another operating the CSLO (Figure 3.1). Contact lenses were not required and no topical or systemic anesthesia was applied. The imaging was stopped for 10 seconds after every 15 seconds to allow eye blinking and keeping the corneal surface moist. The pilot study demonstrated that no photobleaching or phototoxicity was observed imaging at the same laser intensity for 30 minutes considering the morphology of dendrities, axons and cell bodies.

3.2.2 Optic nerve crush

Surgery was carried out under general anaesthesia with a mixture of ketamine ((100 mg/ml) and xylazine (20 mg/ml) (58ug ketamine+8.3ug xylazine) per gram of body weight). Limbal conjunctiva was cut open in the superior region. The sclera was exposed, followed by gentle dissection of periocular blood sinuses, muscle bundles and fatty tissue. Care was taken to avoid bleeding. Optic nerve was then exposed through the small window between surrounding connective tissue. The optic nerve was crushed by the tips of a fine forcept for 5 seconds. Antibiotic ointment was tropically applied after surgery.

3.2.3 Acute elevation of intraocular pressure

Surgery was carried out under general anaesthesia as described in 3.2.2. Stereotaxic instrument was modified to introduce an anterior chamber infusion (Figure 3.2). A micro-injection glass pipette was fixed at the manipulating arm of the SR-6N stereotaxic instrument (Narishige Scientific Instrument Laboratory, Tokyo, Japan). The pipette was connected to a container with 500 ml sterile normal saline. The container was raised to

elevate the IOP to 110 mmHg.

3.2.4 Intravitreal injection of N-methyl-D-aspartic acid (NMDA)

Intravitreal injections were performed under a microsurgical microscope (Zeiss, Jena, Germany) using microinjection syringe (GASTIGHT® Syringe Model 1701, 10μL, Hamilton Co.) connected with a microinjection glass pipette. Mice were anaesthetized with xylazine and ketamine as described in 3.1.1. The ocular surface was disinfected by tropical iodine, followed by rinsing with BSS. Superior conjunctiva was cut open using microscissor (66 vision, Hangzhou, China), followed by the expose of sclera. Glass pipette was injected into sclera at about 1mm behind the limbus. 1 μl of 40mM NDMA (Sigma-Aldrich, St. Louis, MO) prepared in PBS was injected. Care was taken to avoid injury to the lens. The tip of glass pipette stayed in eyeball for about 15s to avoid leakage and allow sufficient time for diffusion inside the vitreous.

3.2.5 In vivo retinal ganglion cell morphometry

The CSLO images were exported to a computer for image analysis using a program written under MATLAB R2007a (The MathWorks, Inc., Natick, Massachusetts, USA) computing language environment. The following 8 parameters (under optic nerve crush model) were measured: 1 cell body area – the area bounded by the cell body contour, 2 axon diameter – the thickness of the axon segments nearest to the cell body, 3 dendritic field – the area bounded by connected line segments joining the ends of all the terminal dendritic branches, 4 number of terminal branches – total number of terminal dendritic ends, 5 total dendritic branch length – the sum of the lengths of all dendrites, 6 distance from the optic disc, 7 branching complexity (modified Sholl Analysis (Ristanovic et al., 2006)) –

traverses of a series of concentric circles with increasing radii were drawn at the center of the cell body, and 8 symmetry. Branching complexity was measured as the mean of the function N(r) representing the number of intersections of the skeletonized dendrites (N) for each of the concentric circles with radius (r). Symmetry was the distance between cell body and dendritic arbor centers of mass / dendritic arbor average radius. Good measurement reliability was found in all 8 parameters with intraclass correlation coefficients ranged between 0.928 and 0.998. Retinal image calibration was based on a schematic eye model for the C57BL / 6J mouse derived by Remtulla and Hallett (Remtulla and Hallett, 1985). It was estimated that 1 degree of field is subtended by 30 μm of retina at $\lambda = 488$nm.

3.2.6 Cluster analysis

Cluster analysis was performed with SPSS 16.0 (SPSS Inc. Chicago, April, 2008). Natural log transformation was used when the morphological parameters were not normally distributed. Parameters were then standardized using the z scores to minimize the effect of differences in measurement scales. Ward's method was used to define the sum of squared Euclidean distances between RGCs. The optimal grouping in the classification was identified with agglomeration coefficient. The survival function of the 6 RGC clusters was evaluated by the Kaplan-Meier estimator and compared with the log–rank test after animal stratification. Baseline morphological parameters were analyzed with the Cox proportional hazards regression model to determine the predictors of RGC survival (Due to collinearity, total dendritic branch length and dendritic field were analyzed separately). As the survival response of individual RGCs is unlikely to be independent within a mouse, a share frailty model was used to adjust for the effect of within-animal correlation. The completely disappearance of fluorescent signal was regarded as the endpoint of RGC survival.

3.2.7 Estimation of dendritic shrinkage rate

STATA (STATA/IC 10.0 for Windows) was used for analysis of dendritic shrinkage. Linear mixed modeling was used to estimate the rate of dendritic shrinkage. With random intercepts and random effects at both the mouse and the eye levels (eye nested within mouse) for the effect of time, the model was fitted with fixed coefficients on baseline dendritic field, age at the time of optic nerve crush, follow-up time, distance away from the optic disc, and the interaction between follow-up time and baseline dendritic field, and distance from the optic disc. In retinal ischemia, the same model was used to estimate the rate of change of dendritic shrinkage and dendritic complexity after 90 minutes of ischemia. With random intercepts and random effects at both the mouse and the eye levels for the effect of time, the model was fitted with fixed coefficients on follow-up time. $P<0.05$ is considered to be statistically significant in all statistical analyses.

3.2.8 Confocal laser scanning microscopy on retinal whole mount

Mice were anesthetized with overdose intraperitoneal injection of dorminal solution (20% W/V) and perfused with PBS. Transcardial perfusion was then performed with 4.0% paraformaldehyde in PBS buffer at pH 7.4. Retinas were dissected after identifying the inferior area of the retina by the inferior position of the ophthalmic artery. They were placed in fixative for 1 hour, rinsed in PBS, and then mounted flat on a glass slide. The retinas were mounted in GB-mount (Golden Bridge Life Science). The RGCs were imaged at 20X or 40 X using a confocal laser scanning microscope (Nikon C1 Confocoal system, Tokyo, Japan).

3.2.9 Immunochemical staining for retinal ganglion cells

The mice were sacrificed after anesthesia with method mentioned in 3.2.9 and perfused with PBS followed by 4% paraformaldehyde. The retinas were diseected out and fixed in 4% paraformaldhyde for 1 hour. The retinas were incubated in a blocking solution containing 10% normal goat serum (NGS), 2% bovine serum albumin (BSA), and 0.5% Triton X-100 in phosphate-buffered saline (PBS; pH 7.4). The primary antibody in 1:100 (anti-SMI-32R antibody) or 1:400 (anti-beta-tubulin TUJ1 antibody) was diluted in 5% NGS, 1% BSA, 0.3% Triton X-100 in PBS and applied for 2 days or 1 day in 4 ℃. Secondary antibody conjugated with rhodamine red or Alex fluroa 488 (1:400) was applied for 2 hours. The retinas were mounted in GB-mount (Golden Bridge Life Science). The number of TUJ1 positive RGCs was counted from 30-40 fields, each measuring 0.25 × 0.25 mm^2, for each eye.

3.2.10 Immunochemical staining for microglia

The retinas were incubated in a blocking solution containing 10% fetal bovine serum (FBS), 0.5% Triton X-100 in PBS (PH 7.4). The primary antibody Iba1 was diluted 1:400 in 5% FBS, 0.4% Triton X-100. Retina was incubated in primary antibody overnight in 4 ℃. Secondary antibody conjugated with Rhodamine red (1:400) was applied for 2 hours. The retinas were mounted in GB-mount (Golden Bridge Life Science).

3.2.11 Longitudinal analysis of microglia proliferation

The CSLO images of the $CX3CR1^{GFP/+}$ mice captured at baseline and then weekly for the first 4 weeks, and monthly thereafter, after optic nerve crush and retinal ischemic injury were exported to a computer for microglia counting using Photoshop (Adobe

Photoshp 7.0). In each retina, 4 rectangular regions, each measuring 400μm x 400μm, were analyzed. The same retinal regions in each eye before and after the injury were selected for serial counting. The activated microglia time curve was constructed with y-axis representing the number of fold of increase in microglia number and x-axis representing the time after the injury. The association between microglia activation and RGC survival was evaluated with a linear regression analysis between the area under the activated microglia time curve and the number of TUJ1 postive RGCs measured at 4 weeks after the injury.

Chapter Four

Results

4.1 *In vivo* imaging of dendritic and axonal arborizations

4.1.1 In vivo imaging of RGC with CSLO

The 488 nm optically pumped semiconductor laser in the confocal scanning laser ophthalmoscope (CSLO) (HRA2, Heidelberg Engineering, GmbH, Dossenheim, Germany) was used to detect the fluorescent signal in the RGCs (488 nm excitation, 500 nm detection). The imaging procedure was performed with one technician gently holding the animal and another operating the CSLO. Contact lenses were not required and no topical or systemic anesthesia was applied. A retinal montage constructed from 12 image captures is shown in (Figure 4.1a). Although the microglia and displaced amacrine cells may exhibit dendritic structures similar to the RGCs, the fluorescent cells can be unambiguously identified as the RGCs since the axons are clearly visible emerging from the cell bodies and converging toward the optic disc. The number and the branching of dendritic arborization imaged by the CSLO has direct correspondence with those observed in retinal wholemount using a confocal scanning laser microscope (Figure 4.1b) although the orientation and spatial arrangement of dendritic trees appeared slightly different. This could be related to changes in tissue architectures during dissection and processing of the retina. The *in vivo* imaging technique provides real-time morphometry of live RGCs which is not possible with conventional histological analysis.

4.1.2 Classification of RGCs

A total of 125 RGCs from 16 retinas with clear axonal and dendritic structures visualized by the CSLO were analyzed. Cluster analysis identified 6 groups of RGCs (Figure 4.2) with reference to 8 morphological and anatomical parameters (cell body size, axonal diameter, dendritic field size, ending branch number, total dendritic branch length,

symmetry, branching complexity (Sholl analysis), and distance from the optic disc) (Figure 4.2). Group 4 RGCs generally had a large dendritic field (148,678 ± 36,853 μm^2, mean ± SD) and soma size (3,180 ± 940 μm^2), long total dendritic branch length (4,164 ± 870 μm), and were located distant from the optic disc (2,020 ± 426 μm) compared with other cell groups. Although there is no consensus on the morphological criteria for RGC classification, most classification systems have been based on measurement of dendritic field and soma size (Boycott and Wassle, 1974; Perry, 1979; Stone and Clarke, 1980; Doi et al., 1995; Sun et al., 2002a; Coombs et al., 2006). With large soma size and dendrites covering a wide area, group 4 RGCs have close resemblance to alpha-cells originally described by Boycott and Wassle in cats (Boycott and Wassle, 1974). For RGCs in groups 5 and 6, the dendritic field (37,285 ± 15,562 μm^2 and 36,380 ± 11,615 μm^2, respectively) and the number of ending dendritic branches (17.3 ± 3.9 and 16.7 ± 3.4) were the smallest, the total dendritic branch length was the shortest (1,608 ± 532 μm and 1,617 ± 336 μm), and the dendritic branching was the least complex. Group 6 RGCs had smaller soma size (1,033 ± 293 μm^2) and were located closer to the optic disc (731.1 ± 364.9μm). These morphological characteristics were similar to those reported in gamma-cells. The dendrites of beta-cells ramify frequently and cover a relatively smaller area (Boycott and Wassle, 1974). These features were found in group 1 RGCs in which they had a medium-sized dendritic field (89,988 ± 26,457 μm^2), yet also had an increased number of ending branches (28.6 ± 4.7) and high branching complexity. The morphological measurements were similar in group 2 and 3 RGCs except the axon diameter, dendritic field and cell body size were generally larger for RGCs in group 3. Most RGCs selected in the analysis belonged to group 5 (33.6%) whereas group 4 RGCs were the least in number (4.0%) (Figure 4.3).

4.1.3 Morphological changes of RGC after optic nerve crush

To study the morphological changes in degenerating RGCs, optic nerve crush was performed. The retinas were serially imaged every other day in the first 4 weeks and at least every week thereafter for 3 to 6 months. Most RGCs demonstrated progressive dendritic shrinkage followed by loss of the axons and the cell bodies (n=84, 68.3%) (Figure 4.4a). Some RGCs had cell bodies detectable for more than 1 to 3 months in the absence of dendritic and axonal structures (n=9, 7.3%) (Figure 4.4b). A significant proportion of RGCs (n=26, 21.1%) showed only partial loss of dendritic structures without loss of the axons and the cell bodies at 6 months after the injury (Figure 4.4c). Immunohistochemical staining with anti-SMI-32 indicated that the dendritic shrinkage was not due to redistribution of cytoplasmic YFP (Figure 4.4d). Progressive axonal changes were only observed in a few RGCs. In 3 RGCs (2.4%), Wallerian degeneration with fragmentation and beading of the axon was observed following progressive dendritic shrinkage (Figure 4.5a). In one RGC (0.8%), the proximal axon showed retraction and bulb formation before cell death (Figure 4.5b).

4.1.4 Predictive factors of RGC survival

Survival analysis showed that group 4 RGCs had the best survival function and group 6 had the worst (Figure 4.6a) (the RGC survival endpoint was defined as complete loss of fluorescent signal). This finding is in agreement with the observation of Watanabe and Fukuda (Watanabe and Fukuda, 2002), which demonstrated that alpha cells have higher abilities to regenerate their axons among axotomized RGCs. There was a significant difference in the survival function between RGCs in group 4 and RGCs in groups 1, 2, 5 and 6 (log-rank test stratified for mouse, p=0.038). Among the 8 morphological parameters

measured at baseline, the dendritic field, total dendritic branch length and distance from the optic disc were independent predictors of RGC survival in the Cox regression analysis (all with $p \leq 0.035$). Improved survival function was generally found in cells with a larger dendritic field, longer total dendritic branch length, and at a longer distance from the optic disc. The probability of survival is increased by 13.1%, 4.4% and 6.0% for every 10,000 μm^2 increase in dendritic field, every 100 μm increase in total dendritic branch length, and every 100 μm increase in distance away from the optic disc, respectively. Baseline cell body size, axon diameter, symmetry, dendritic branching complexity and the number of ending dendritic branches had no association with RGC survival. It is possible to predict the survival probability of individual RGC with reference to baseline morphological measurements. Figure 4.6b compared the predicted survival probability of RGCs with a large (150,000 μm^2) and a small (35,000 μm^2) dendritic field after standardizing other morphological measurements. At one month after optic nerve crush, the survival probabilities were 0.85 and 0.45, respectively. It is plausible that RGCs located further away from the optic disc have a better survival probability as they are more distant from the site of injury. To determine if the site of RGC damage has an effect on survival, direct injury to the RGCs was induced by intravitreal injection of N-methyl-D-aspartic acid (NMDA) (41 RGCs from 4 mice). Similar to optic nerve crush, surviving RGCs at one month after intravitreal injection of NMDA had significantly larger baseline dendritic fields and longer total dendritic branch length ($p<0.001$). However, there was no difference in distance from the optic disc between the surviving and the degenerated RGCs ($p=0.702$). This result indicates that RGCs with larger dendritic field and longer dendritic branch length in general have better survival and that the location of RGC is important to survival only when the injury site is near the optic nerve.

4.1.5 Esimation of rate of dendritic shrinkage after optic nerve crush

A linear mixed model was applied to estimate the rate of change of dendritic field of individual RGCs after optic nerve crush. A total of 673 serial dendritic field measurements from 122 RGCs were analyzed. Interaction terms between the time after the crush and the baseline dendritic field, and the distance from the optic disc were included in the model to evaluate their influences on the rate of dendritic shrinkage. In agreement with the Cox proportional hazards regression analysis, the positive coefficient of the interaction terms ($1.34X10^{-7}$ and $7.60X10^{-6}$, respectively) indicates that RGCs with a larger baseline dendritic field or at a longer distance from the optic disc had a slower rate of dendritic shrinkage. For example, the rate of dendritic shrinkage of a RGC with a dendritic field 10,000 μm^2 and close to the optic nerve head (600 μm) would be -3.51% [-0.041 (coefficient of time in day) x 1 + $1.34x10^{-7}$ x 10,000 + $7.60X10^{-6}$ x 600)] per day. This is in contrast to a RGC with a larger dendritic field (150,000 μm^2) at the same location in which the estimated rate of dendritic shrinkage is -1.63% per day. The average rate of dendritic shrinkage was estimated at -2.00% per day. RGCs with large dendritic field distant from the optic disc have the slowest rate of dendritic shrinkage after optic nerve crush.

4.1.6 Chapter summary

RGC damage was observed prospectively to begin with progressive dendritic shrinkage, followed by loss of the axon and the cell body. In a small proportion of RGCs, progressive axonal changes with fragmentation, beading, retraction and bulb formation were also observed. RGCs with larger dendritic field and longer dendritic branch length in general have better survival probability. The rate of dendritic shrinkage is variable with a slower rate in cells having a large dendritic field, long total dendritic branch length and

being distant from the optic disc.

4.2 Longituidnal profiles of retinal ganglion cell degeneration after ischemic injury induced by elevation of IOP

4.2.1 Morphological changes of RGCs

Thirty-one RGCs from 8 eyes with distinct axonal and dendritic arborization patterns visualized with the CSLO at baseline were randomly selected for longitudinal imaging. They were imaged at baseline, 1-3 days, 7 days, and then every 1-2 weeks for at least 1-3 months after acute elevation of intraocular pressure. Figure 4.7 shows the baseline morphological measurements of the 31 RGCs. The mean dendritic field, dendritic branching complexity, axonal diameter and cell body area were 17770.3μm^2, 9.0 (modified Sholl analysis (Ristanovic et al., 2006)), 4.6μm and 499.0μm^2, and the ranges were 6547.2μm^2 – 49944.2μm^2, 5.448 – 12.325, 2.8μm – 6.6μm, and 260.9μm^2 –1036.2μm^2, respectively.

There were no detectable changes in axonal or dendritic structures after 30 minutes (n=12) (Figure 4.8a) of ischemia. After 90 minutes of ischemia, 78.9% (n=15) of RGCs showed progressive loss of the dendrites, the axon and then the cell body at 1-2 weeks after the injury (Figure 4.8b). Complete loss of dendritic tree was evident as early as day 3 after the injury. 15.8% (n=3) had no detectable changes at 2 months after the injury (Figure 4.8c). In one RGC (5.3%), there was only mild reduction of branching complexity and shrinkage of dendritic field (Figure 4.9). There were no significant differences in the baseline dendritic field, dendritic branching complexity, axonal diameter and cell body area between the 2 groups of RGCs with different duration of retinal ischemia ($p \geq 0.065$).

4.2.2 Rate of change of dendritic field and branching complexity

A total of 136 longitudinal measurements of dendritic field and dendritic complexity were included for estimation of rate of change with linear mixed modeling. There was no significant change in dendritic field and branching complexity after 30 minutes of ischemia ($p \geq 0.674$). After 90 minutes of ischemia, the mean rate of reduction of dendritic field was 11.7% (95% confidence interval: 5.0% - 18.4%) per day, and that of branching complexity was 11.1% (5.0% - 17.2%) per day. The larger baseline dendritic field was significantly associated with a slower rate of dendritic shrinkage ($p=0.002$). A longer duration of ischemic insult was associated with a faster reduction of dendritic field and branching complexity.

Figure 4.9 illustrates the shrinkage of dendritic tree and reduction in branching complexity of an RGC at 107 days after 90 minutes of ischemia. To confirm the morphological changes observed with *in vivo* imaging were not secondary to redistribution of cytoplasmic YFP, the retina was stained with anti-SMI32, an anti-neurofilament antibody. The co-localization between YFP and anti-SMI32 suggests that the *in vivo* CSLO imaging provides a reliable method to track dendritic and axonal changes.

4.2.3 Chapter summary

RGCs have relatively high tolerance to ischemic injury with dendritic shrinkage evident after 30 minutes, but not 90 minutes of retinal ischemia. The rate of dendritic shrinkage of 90 minutes of retinal ischemia (11.7% per day) was faster than that of optic nerve crush (2.0% per day). A larger dendritic field was associated with a smaller rate of dendritic shrinkage.

4.3 *In vivo* imaging of retinal microglia

4.3.1 In vivo morphology of retinal microglia

A total of 18 eyes from 17 $CX3CR1^{GFP/+}$ transgenic mice were serially imaged. The CSLO allows visualization of individual microglial cells although detailed morphology can only be discerned in a small proportion of microglia (Figure 4.10). The density of retinal microglia ranged between 148/mm^2 and 224/mm^2 with a mean of 188/mm^2. The distribution of microglia was regular and there was no spatial difference in cell density ($p>0.100$).

4.3.2 Longitudinal profile of retinal microglia after optic nerve crush and retinal ischemic injury

After optic nerve crush (n=4), there was more than two-fold proliferation of retinal microglia evident at week 1. The number of microglia gradually decline with 2.1+/-0.1, 1.9+/-0.2 and 1.6+/-0.1 fold increase at week 2, 3 and 4, respectively (Figure 4.11) The longitudinal profile of microglia proliferation followed a similar pattern after retinal ischemia induced by elevating the intraocular pressure at 110mmHg with a peak observed at week 1 followed by a gradual decline in the following weeks (Figure 4.11). The increase in cell density was proportional to the duration of ischemia. At week 1, there were 1.3+/-0.1, 1.9+/-0.1, 2.3+/-0.3 and 2.8+/-0.2 fold increase in microglia after 30, 60, 90 and 120 minutes of ischemia, respectively. The differences in microglial proliferation at week 1 were statistically significant ($p<0.001$). Activated microglia time curves showing the longitudinal profiles of microglia proliferation of individual eyes are shown in Figure 4.12. All GFP-labeled cells were Iba-1 positive at baseline, after optic nerve crush and after retinal ischemia (Figure 4.13). The morphologies of microglia changed from ramified form

at baseline to ameboid form when they were activated at week 1 after the injury (Figure 4.14). They were then returned to ramified form in the following weeks.

4.3.3 Association between macrophage activation and RGC death

Animals were sacrificed with retinas dissected at week 4 after optic nerve crush or retinal ischemia for TUJ1 immunohistochemical staining. The number of TUJ1 positive RGCs decreased with increasing duration of ischemia (Figure 4.15). There was a significant association between the number of RGCs surviving at week 4 and the area under the activated microglia time curve ($P<0.001$). Increased area under the activated microglia time curve was associated with reduced number of RGCs (Figure 4.16).

4.3.4 Chapter summary

In vivo imaging of the $CX3CR1^{GFP/+}$ transgenic mice facilitates the investigation of the longitudinal dynamics of retinal microglia activation. Microglia proliferation peaked at 1 week after retinal ischemic or optic nerve crush injury. The proliferation was positively correlated with the degree of injury and negatively correlated with the survival of RGCs. Investigating the activation of microglia could provide mechanistic insight to RGC degeneration.

Chapter Five

Discussion

5.1 *In vivo* CSLO imaging of RGCs

Being able to serially monitor cellular morphology has been a major challenge in studying RGC degeneration. Animal models designed for *in vivo* imaging almost always required systemic anesthesia, which is undesirable for frequent, long term assessment. In addition, clouding of the lens associated with systemic anesthesia could impair visualization of the fundus . Walsh and Quigley demonstrated the feasibility of *in vivo* imaging of dendritic processes of RGCs in anaesthetized Thy1-YFP16Jrs transgenic mice with a modified confocal laser scanning microscope (Walsh and Quigley, 2008). However, dendritic arborization visualized in this model was not as distinct as fixed tissue imaging and this limited the potential for quantitative morphological analysis. Gray et al showed that it is possible to image the dendritic arborization in macaques using an adaptive optics scanning laser ophthalmoscope with retrograde labeling (Gray et al., 2008). However, the labeling with rhodamine is transitory. Long term *in vivo* analysis of dendritic damage in neuronal degeneration has not been demonstrated previously.

The key advantage of this real-time CSLO imaging is that it provides an efficient and non-invasive approach for capturing serial retinal images at the same location over months. In particular, there is consistently high image quality that allows detailed morphological analysis and classification of RGCs, monitoring of axonal and dendritic changes, evaluation of survival probability, and measurement of the rate of dendritic shrinkage. Imaging is performed with gentle holding of the animal without using any local or systemic anesthetic agent, which may compromise animal survival particularly when serial capture is warranted. The feasibility of long term monitoring of dendritic and axonal changes for more than 6 months has been demonstrated in this study (Figure 4.4c). *In vivo* imaging of the Thy-1 YFP has been reported using a confocal scanning laser microscope (Walsh and Quigley, 2008). The advantages of using an CSLO are improved resolution of

dendritic and axonal structures for quantitative analysis and that imaging can be performed while the animal is awake. Different from the Thy-1 CFP strain in which over 95% of RGCs express CFP (Leung et al., 2008b), only a small proportion of RGCs in the Thy-1 YFP mice express fluorescent protein. For this reason, the dendritic trees and axon of individual neurons can be discriminated and visualized in the Thy-1 YFP mice. The disparity in the expression pattern has been proposed to be related to position effect variegation and repeat-induced gene silencing (Feng et al., 2000). Of note, the YFP expressing RGCs likely represent a random sample of the retina as it has been shown that the expression has no predilection for specific subtypes of RGCs (Coombs et al., 2006). While the trade-off in visualizing dendritic and axonal morphologies is losing information on cell density, cross-breeding of Thy-1 CFP and Thy-1 YFP mice and using a dual laser system in the CSLO to capture both cyan and yellow fluorescent signals would be useful to collect both information in the same animal.

5.2 The limitations of CSLO imaging

The confocal imaging technique, however, is limited in evaluating the dendritic stratification in cross-section. It is not yet possible to identify the dendritic spines with the current instrumentation. This information was not available for the cluster analysis thereby limiting finer classification. Nevertheless, it is evident from the Kaplan Meier analysis that the current morphological classification is related to RGC survival (Figure 4.6a). In fact, we are able to predict the survival probability and estimate the rate of dendritic shrinkage after optic nerve crush based on the size of dendritic field and the distance from the optic disc measured at baseline. Considering the different pattern of dendritic stratification of ON- and OFF-RGCs, it would be greatly significant if we can differentiate ON- and OFF-RGCs through enhancing the z-axis resulotion of *in vivo* imaging. Development of lens opacity is

common following general anesthesia in mice (Leung et al., 2009). In this study, imaging was performed without using any local or systemic anesthetic agent. The natural blinking reflex would prevent corneal drying and worsening of image quality. Imaging could thus be conducted repetitively and longitudinally for months without compromising the optical media or survival of the animal. The co-localization of anti-SMI32 antibodies and YFP in degenerating dendritic trees indicated that loss of fluorescent signals detected *in vivo* likely represents loss of dendrites but not redistribution of cytoplasmic YFP. Although laser exposure during repeated imaging may theoretically bleach and reduce the intensity of fluorescent signal of RGCs, no change in fluorescent signal was observed in eyes undergoing 30 minutes of ischemia when they had the same intensity and duration of laser exposure compared to those after a longer duration of ischemia. This finding indicates that CSLO imaging is safe and effective to follow morphological changes of RGCs.

It should be noted that, the RGC soma diameter calculated out in this study is 53-72μm in group 4 and 31-41μm in group 6, which is much larger than soma diameter demonstrated by previous studies, including Sun (7-33 μm) (Sun et al., 2002a) and Coombs (<28 μm) (Coombs et al., 2006; Coombs et al., 2007). This variation maybe derived from the difference of RGC morphometry. The morphological analyses in those studies were performed in vitro; however, it is very possible that the somas underwent shrinkage during the fixation. The laser light scatter during *in vivo* imaging is another possible reason for the large soma size demonstrated in this study.

5.3 Significance of following dendritic shrinkage and axonal degeneration

To our knowledge, this is the first study measuring and modeling progressive dendritic shrinkage *in vivo*. We showed that RGC degeneration began with the dendritic trees, followed by loss of the axons and finally the cell bodies (Figure 4.8b). The rate and the degree of dendritic shrinkage, however, were variable among individual neurons. RGCs

with larger dendritic field showed a higher survival probability and a slower rate of dendritic shrinkage.

It is notable that progressive axonal changes were only observed in a small proportion of RGCs, suggesting that axonal degeneration is a relatively rapid process. It has been proposed that focal axonal lesions induce Wallerian degeneration of distal axons whereas the proximal axons "die back". Using the Thy-1 GFP-S transgenic mice, Kerschensteiner et al showed that spinal cord axons underwent acute axonal degeneration with rapid retraction of proximal axon stumps within 30 minutes after transection followed by Wallerian degeneration of distal axons after 30 hours (Kerschensteiner et al., 2005). In this study, we found that both Wallerian degeneration (Figure 4.5a) and axonal retraction (Figure 4.5b) could take place in proximal axons. And this could occur even at a month after optic nerve crush. While the mechanism triggering the axonal degeneration remains to be elucidated, a common molecular pathway involving Wallerian degeneration slow (WLD-S) has been suggested for Wallerian degeneration and axonal retraction (Lunn et al., 1989; Kerschensteiner et al., 2005). The delayed axonal degeneration in the RGCs implies a potential therapeutic window after optic nerve injury. In some RGCs, the cell bodies survived despite the absence of detectable axons and dendritic arborization (Figure 4.4b). Restoring axonal and dendritic structures would be a key area for research on neuronal regeneration. It has been demonstrated that axon degeneration precedes cell death in neurodegenerative diseases (Li et al., 2001; Stokin et al., 2005). We found that dendritic shrinkage could be evident even before axon degeneration and could thus serve as an early sign for neuronal damage. Being able to visualize the changes in dendritic arborization and measure the rate of dendritic shrinkage provides a new paradigm to study the mechanism of neurodegeneration and may provide new insights in testing novel therapies for neuroprotection.

5.4 Monitoring dendritic shrinkage as a biomarker for the health of RGCs

We showed that the RGCs have relatively high tolerance of retinal ischemia. Even when the IOP was elevated to 110 mmHg for 30 minutes, there were no detectable changes in dendritic and axonal arborization. After 90 minutes of high IOP elevation, a significant proportion of RGCs showed progressive shrinkage of dendritic trees followed by loss of the axon and then the cell body. With longitudinal measurement of dendritic field, the rate of dendritic shrinkage was estimated at 11.7% per day after 90 minutes of ischemia. The ability to visualize and track dendritic changes could provide a sensitive approach to evaluate the health of RGCs.

There is a paucity of published data reporting the morphologies of RGCs after elevation of intraocular pressure. Prior studies have been derived from histological examination of retinas dissected after the injury. In the study by Weber et al. using a primate model of experimental glaucoma and intracellular staining of RGCs with Lucifer yellow, the earliest sign of RGC degeneration detected was a change in the dendritic arborization (Weber et al., 1998). Similar observation of dendritic pruning in human glaucoma was also reported by Pavlidis et al. with intraretinal labeling in enucleated eyes (Pavlidis et al., 2003). It has been suggested that RGCs with larger soma and larger dendritic field were more tolerant to dendritic damage and cell loss after acute intraocular pressure elevation (Shou and Zhou, 1989). In contrast, they were more susceptible to damage after chronic intraocular pressure elevation (Quigley et al., 1987; Quigley et al., 1988; Glovinsky et al., 1991). Observation from histological studies, however, is always limited at a single time point. It is impossible to know whether the dendritic arborization had changed without visualizing their morphologies at baseline. In addition, changes in dendritic and axonal structures could be related to severing of the axons during dissection

of the retina. A group of normal controls is therefore always needed for comparison in histological studies. With high resolution *in vivo* imaging, we were able to demonstrate that degeneration of RGCs begins with dendritic shrinkage and that the rate of dendritic shrinkage was associated with the size of dendritic field measured at baseline. Similar to optic crush, RGCs with a larger dendritic field had a slower rate of dendritic shrinkage after retinal ischemic injury. Remarkably, there were no morphological changes in the dendritic and axonal arborization after 30 minutes of ischemia (Figure 4.8a). Even after 90 minutes of ischemia, a significant proportion of RGCs survived with intact dendritic and axonal structures (Figure 4.8c). These results concur with our previous investigation using the blue-light CSLO to measure the number of RGC after acute intraocular pressure elevation (Leung et al., 2009). A reduction in RGC number (14.5% - 79.5% reduction relative to baseline measurement) was observed only after 90 minutes, but not after 45 minutes of ischemia. The ability to follow dendritic and axonal morphologies further supports the notion that structural damage would not be evident with a short period of ischemia. The good maintenance of the structural integrity of RGCs to ischemic injury has been attributed to the considerable amounts of glucose in the vitreous and the capacity to extract ATP from glycolysis (Kuwabara and Cogan, 1961; Osborne et al., 2004). In contrast to the generally well-preserved structural integrity, functional impairment could be detected after a short duration of ischemia. It has been shown that there was complete, reversible loss of scotopic ERG b-wave even after only 4 minutes of ischemia (Osborne et al., 2004). In such a model system, functional changes of RGCs likely precede structural damage in retinal ischemia.

Of note, the conventional approach of counting the cell body may not as sensitive as measuring the rate of dendritic shrinkage as an indicator of RGC damage. As shown in figure 4.8b (after retinal ischemic injury) and figure 4.4b (after optic nerve crush), the presence of the cell body does not represent an intact RGC. The mean rate of dendritic

shrinkage was 2.00% per day after optic nerve crush and 11.7% per day after 90 minutes of ischemia. Treatment may be effective to preserve RGC function if initiated at a stage before complete loss of dendritic tree. The ability to monitor dendritic and axonal arborization thereby provides a sensitive approach to identify a potential therapeutic window for neuroprotective treatment.

5.5 Dynamic profile of microglia activation

Investigating the time course of microglia activation following optic nerve and retinal ischemic injury is pertinent in providing mechanistic insight of RGC degeneration. Using an CSLO to image the CX3CR1$^{GFP/+}$ transgenic mice, we demonstrated the dynamic changes of retinal microglia after optic nerve crush and acute elevation of intraocular pressure. The number of retinal microglia increased with a peak observed at 1 week after the injury which was followed by a gradual decline approaching near to the baseline at 4 weeks. The activation of retinal microglia was proportional to the duration of retinal ischemic injury with a range between 1.3-fold and 2.8-fold increase in cell number after 30 minutes and 120 minutes of ischemia, respectively. The number of RGCs measured at 4 weeks post-injury was significantly associated with the number of activated retinal microglia.

CSLO imaging of the CX3CR1$^{GFP/+}$ transgenic mice is an efficient approach to visualize the dynamic changes of retinal microglia. Although CX3CR1 can also be expressed by hematopoietic cells, NK cells, Th1 lymphocytes, and CD14+ monocytes (Marchesi et al., 2010), the co-localization between CX3CR1 and Iba-1 in both resting and activated states confirmed the identity of the fluorescent cells we imaged were essentially microglia. The key advantage of using an CSLO over an CSLM is the feasibility to perform *in vivo* imaging thereby permitting long term monitoring of microglial changes.

This merit, however, is at the expense of a lower image resolution compared to CSLM imaging on retinal explants. While it is possible to differentiate the ramified form from the ameboid form of microglia with our *in vivo* CSLO image capture (Figure 4.14), detailed morphology of individual cellular processes cannot be discerned.

5.6 Association between microglia activation and RGC survival

Retinal microglia are resident macrophages that have been implicated in phagocytosis, antigen presentation and secretion of various cytokines and growth factors (Gupta et al., 2003; Langmann, 2007) Their activation after optic nerve or retinal injury is closely related to the survival of RGCs. Although it has been recognized that retinal microglia increase in number and transform from ramified to ameoboid form when they are activated, their dynamic profiles of activation in relation to the degree of insult and RGC damage have not been investigated. This is because of the lack of reliable model systems that provide serial monitoring of individual microglial cell. CSLO imaging of the $CX3CR1^{GFP/+}$ transgenic mice allows precise measurement of the number of microglia *in vivo* thereby facilitating comparison before and after activation in the same eyes. An important finding in the study is that microglia proliferation peaked at approximately one week independent of the form and the degree of injury (Figure 4.12).

Understanding the longitudinal dynamic of microglial activation is germane to the investigation of neuroprotection because it has been demonstrated that the magnitude of RGC protection and axon regeneration depends upon the timing and extent of macrophage influx (Yin et al., 2003). Secreting both positive- (e.g. BDNF, GDNF) and negative-acting factors (e.g. TNF-α, IL-1β) (Langmann, 2007), microglia can exert both protective and deleterious effect on RGCs. The net effect could be related to the timing of microglia activation. Yin et al. showed that activating macrophages with Zymosan 3 days, but not 1

week after optic nerve crush, promoted regeneration of RGC axons (Yin et al., 2003). The close association between microglial activation and RGC survival is also reflected from the finding that the degree of proliferation was proportional to the duration of ischemia. Retina with 30, 60, 90 and 120 minutes of ischemia had 1.3-, 1.9-, 2.3- and 2.8- fold increase in microglia at week 1, respectively. Of note, despite the number of activated microglia measured at one week was more for eyes after 120 minutes of ischemia than those after optic nerve crush, the number of RGCs survived at 1 month was the least after optic nerve crush (Figure 4.15). It is important to recognize activated microglia in fact persisted for a longer period after optic nerve crush and that the area under the activated microglia time curve was the largest. There was a significant negative correlation between the area under the activated microglia time curve and the number of surviving RGCs. While the molecular mechanism of microglial activation in relation to RGC degeneration is not entirely clear, CX3CR1 signaling likely plays a significant role in mediating RGC death. CX3CR1 is expressed by the retinal microglia and functions as a chemotactic receptor for fractalkine, which has been implicated in the control of microglial neurotoxicity (Jung et al., 2000; Meucci et al., 2000). In a recent study by Fuhrmann et al using two-photon *in vivo* imaging, knocking out the microglial chemokine receptor CX3CR1 has been shown to prevent neuron loss in a mice model of Alzheimer's disease (Fuhrmann et al., 2010). Modifying the signaling pathway of CX3CR1 could be a potential therapeutic target to enhance RGC survival.

It is notable that despite there was no detectable loss of RGCs after 30 minutes of retinal ischemia, there was a significant increase in microglial cells 1 week after the injury. In a previous *in vivo* imaging study on the Thy-1 CFP transgenic mice, we showed that there was no loss of Thy-1 expressing RGC after 45 minutes of ischemia (Leung et al., 2009). Yet, damage to the RGCs might have incurred as it has been shown that there was

complete, reversible loss of scotopic ERG b-wave even after only 4 minutes of ischemia (Osborne et al., 2004). Imaging microglia activation may thus provide a sensitive approach to detect potential RGC damage or dysfunction.

5.7 Conclusion

In this study, we used two experimental models based on *in vivo* imaging of retinal ganglion cells and microglial cells in the Thy-1 YFP mice and the CX3CR1+/GFP mice to investigate the longitudinal profiles of axonal and dendritic damage and microglia activation following retinal ganglion cell degeneration induced by optic nerve crush and acute elevation of intraocular pressure. The reliability of *in vivo* imaging of RGCs is evident by the clear visualization of axonal and dendritic arborizations of individual neurons. Morphological parameters including dendritic field size and dendritic branching comlexity could be precisely measured in this study. Although the dendritic structure of microglia observed *in vivo* was not as clear as that imaged with a confocal scanning laser microscope, it is still possible to differentiate the ramified form from the ameboid form. To our knowledge, this is the first study demonstrating *in vivo* measurement of the rate of dendritic shrinkage and microglia proliferation following optic nerve and retinal ischemic injury. The co-localization of YFP and anti-SMI32, and GFP and IBa-1 in the retinal flatmount confirms the identities of the fluorescent cells discerned in the *in vivo* images are RGCs and microglia, respectively.

We observed that the patterns of axonal and dendritic degeneration were diverse. There were wallerian degeneration, axonal retraction, shrinkage of dendritic trees and reduction in branching complexity following optic nerve injury. The rate of dendritic shrinkage was estiatmed at 2.0% per day after optic nerve crush and 11.7% per day after 90 minutes of retinal ischemia. RGCs with larger dendritic field had higher probability of

survival after injury. These findings provide the foundation to investigate the molecular mechanisms of RGC degeneration, identify potential windows for therapeutic intervention, and evaluate the safety and effectiveness of neuroprotective agents. The finding of a significant association between microglia profileration and reduced RGC survival following optic nerve and retinal ischemic injury supports further investigation in the CX3CR1 signaling pathway in relation to RGC degeneration.

Future studies will be planned to screen and identify potential neuroprotective agents for various types of optic neuropathy including glaucoma. Measuring and following dendritic shrinkage allows a fast and efficient approach to detect small treatment effects without sacrificing a large number of animals. Cross-breeding of the Thy-1 YFP and CX3CR1 transgenice mice will provide a unique model to study the longitudinal interaction between micoglia and RGCs and investigate the activation and suppression of microglia in relation to dendritic and axonl changes of RGCs.

References

Amthor FR, Oyster CW, Takahashi ES (1983) Quantitative morphology of rabbit retinal ganglion cells. Proc R Soc Lond B Biol Sci 217:341-355.

Avramut M, Achim CL (2003) Immunophilins in nervous system degeneration and regeneration. Curr Top Med Chem 3:1376-1382.

Badea TC, Nathans J (2004) Quantitative analysis of neuronal morphologies in the mouse retina visualized by using a genetically directed reporter. J Comp Neurol 480:331-351.

Barnstable CJ, Drager UC (1984) Thy-1 antigen: a ganglion cell specific marker in rodent retina. Neuroscience 11:847-855.

Barron KD (1995) The microglial cell. A historical review. J Neurol Sci 134 Suppl:57-68.

Batchelor PE, Liberatore GT, Wong JY, Porritt MJ, Frerichs F, Donnan GA, Howells DW (1999) Activated macrophages and microglia induce dopaminergic sprouting in the injured striatum and express brain-derived neurotrophic factor and glial cell line-derived neurotrophic factor. J Neurosci 19:1708-1716.

Bechmann I, Priller J, Kovac A, Bontert M, Wehner T, Klett FF, Bohsung J, Stuschke M, Dirnagl U, Nitsch R (2001) Immune surveillance of mouse brain perivascular spaces by blood-borne macrophages. Eur J Neurosci 14:1651-1658.

Beirowski B, Adalbert R, Wagner D, Grumme DS, Addicks K, Ribchester RR, Coleman MP (2005) The progressive nature of Wallerian degeneration in wild-type and slow

Wallerian degeneration (WldS) nerves. BMC Neurosci 6:6.

Bernier B, Castejon S, Culver DG, Glass JD (1999) Axonal neurofilaments are resistant to calpain-mediated degradation in the WLD(S) mouse. Neuroreport 10:1423-1426.

Berson DM, Dunn FA, Takao M (2002) Phototransduction by retinal ganglion cells that set the circadian clock. Science 295:1070-1073.

Beuche W, Friede RL (1986) Myelin phagocytosis in Wallerian degeneration of peripheral nerves depends on silica-sensitive, bg/bg-negative and Fc-positive monocytes. Brain Res 378:97-106.

Bomstein Y, Marder JB, Vitner K, Smirnov I, Lisaey G, Butovsky O, Fulga V, Yoles E (2003) Features of skin-coincubated macrophages that promote recovery from spinal cord injury. J Neuroimmunol 142:10-16.

Bouhy D, Malgrange B, Multon S, Poirrier AL, Scholtes F, Schoenen J, Franzen R (2006) Delayed GM-CSF treatment stimulates axonal regeneration and functional recovery in paraplegic rats via an increased BDNF expression by endogenous macrophages. FASEB J 20:1239-1241.

Bouldin TW, Cavanagh JB (1979) Organophosphorous neuropathy. I. A teased-fiber study of the spatio-temporal spread of axonal degeneraion. Am J Pathol 94:241-252.

Boycott BB, Wassle H (1974) The morphological types of ganglion cells of the domestic cat's retina. J Physiol 240:397-419.

Boycott BB, Hopkins JM (1981) Microglia in the retina of monkey and other mammals: its distinction from other types of glia and horizontal cells. Neuroscience 6:679-688.

Brown AM, Westenbroek RE, Catterall WA, Ransom BR (2001) Axonal L-type Ca2+

channels and anoxic injury in rat CNS white matter. J Neurophysiol 85:900-911.

Bruck W, Friede RL (1991) The role of complement in myelin phagocytosis during PNS wallerian degeneration. J Neurol Sci 103:182-187.

Bruck W, Bruck Y, Friede RL (1992) TNF-alpha suppresses CR3-mediated myelin removal by macrophages. J Neuroimmunol 38:9-17.

Bruck W, Bruck Y, Maruschak B, Friede RL (1995) Mechanisms of macrophage recruitment in Wallerian degeneration. Acta Neuropathol 89:363-367.

Buchi ER, Suivaizdis I, Fu J (1991) Pressure-induced retinal ischemia in rats: an experimental model for quantitative study. Ophthalmologica 203:138-147.

Buki A, Povlishock JT (2006) All roads lead to disconnection?--Traumatic axonal injury revisited. Acta Neurochir (Wien) 148:181-193; discussion 193-184.

Buki A, Okonkwo DO, Wang KK, Povlishock JT (2000) Cytochrome c release and caspase activation in traumatic axonal injury. J Neurosci 20:2825-2834.

Calderone L, Grimes P, Shalev M (1986) Acute reversible cataract induced by xylazine and by ketamine-xylazine anesthesia in rats and mice. Exp Eye Res 42:331-337.

Callaway EM (2005) Structure and function of parallel pathways in the primate early visual system. J Physiol 566:13-19.

Carcieri SM, Jacobs AL, Nirenberg S (2003) Classification of retinal ganglion cells: a statistical approach. J Neurophysiol 90:1704-1713.

Castano A, Bell MD, Perry VH (1996) Unusual aspects of inflammation in the nervous system: Wallerian degeneration. Neurobiol Aging 17:745-751.

Cavanagh JB (1979) The 'dying back' process. A common denominator in many naturally occurring and toxic neuropathies. Arch Pathol Lab Med 103:659-664.

Chen L, Yang P, Kijlstra A (2002) Distribution, markers, and functions of retinal microglia. Ocul Immunol Inflamm 10:27-39.

Coombs J, van der List D, Wang GY, Chalupa LM (2006) Morphological properties of mouse retinal ganglion cells. Neuroscience 140:123-136.

Coombs JL, Van Der List D, Chalupa LM (2007) Morphological properties of mouse retinal ganglion cells during postnatal development. J Comp Neurol 503:803-814.

Cordeiro MF, Guo L, Luong V, Harding G, Wang W, Jones HE, Moss SE, Sillito AM, Fitzke FW (2004) Real-time imaging of single nerve cell apoptosis in retinal neurodegeneration. Proc Natl Acad Sci U S A 101:13352-13356.

Dacey DM, Peterson BB, Robinson FR, Gamlin PD (2003) Fireworks in the primate retina: in vitro photodynamics reveals diverse LGN-projecting ganglion cell types. Neuron 37:15-27.

Davalos D, Grutzendler J, Yang G, Kim JV, Zuo Y, Jung S, Littman DR, Dustin ML, Gan WB (2005) ATP mediates rapid microglial response to local brain injury in vivo. Nat Neurosci 8:752-758.

Doi M, Uji Y, Yamamura H (1995) Morphological classification of retinal ganglion cells in mice. J Comp Neurol 356:368-386.

Eter N, Engel DR, Meyer L, Helb HM, Roth F, Maurer J, Holz FG, Kurts C (2008) In vivo visualization of dendritic cells, macrophages, and microglial cells responding to laser-induced damage in the fundus of the eye. Invest Ophthalmol Vis Sci 49:3649-3658.

Feng G, Mellor RH, Bernstein M, Keller-Peck C, Nguyen QT, Wallace M, Nerbonne JM, Lichtman JW, Sanes JR (2000) Imaging neuronal subsets in transgenic mice expressing multiple spectral variants of GFP. Neuron 28:41-51.

Fiala JC, Spacek J, Harris KM (2002) Dendritic spine pathology: cause or consequence of neurological disorders? Brain Res Brain Res Rev 39:29-54.

Fuhrmann M, Bittner T, Jung CK, Burgold S, Page RM, Mitteregger G, Haass C, LaFerla FM, Kretzschmar H, Herms J (2010) Microglial Cx3cr1 knockout prevents neuron loss in a mouse model of Alzheimer's disease. Nat Neurosci 13:411-413.

Garbarino-Pico E, Carpentieri AR, Contin MA, Sarmiento MI, Brocco MA, Panzetta P, Rosenstein RE, Caputto BL, Guido ME (2004) Retinal ganglion cells are autonomous circadian oscillators synthesizing N-acetylserotonin during the day. J Biol Chem 279:51172-51181.

Gelbard HA (2004) Synapses and Sisyphus: life without paraplegin. J Clin Invest 113:185-187.

George R, Griffin JW (1994) The proximo-distal spread of axonal degeneration in the dorsal columns of the rat. J Neurocytol 23:657-667.

Gillingwater TH, Ribchester RR (2003) The relationship of neuromuscular synapse elimination to synaptic degeneration and pathology: insights from WldS and other mutant mice. J Neurocytol 32:863-881.

Gillingwater TH, Thomson D, Mack TG, Soffin EM, Mattison RJ, Coleman MP, Ribchester RR (2002) Age-dependent synapse withdrawal at axotomised neuromuscular junctions in Wld(s) mutant and Ube4b/Nmnat transgenic mice. J Physiol 543:739-755.

Glass JD, Brushart TM, George EB, Griffin JW (1993) Prolonged survival of transected nerve fibres in C57BL/Ola mice is an intrinsic characteristic of the axon. J Neurocytol 22:311-321.

Glovinsky Y, Quigley HA, Dunkelberger GR (1991) Retinal ganglion cell loss is size dependent in experimental glaucoma. Invest Ophthalmol Vis Sci 32:484-491.

Graeber M, Blakemore W, Kreutzberg GW (2002) Cellular pathology. In: Greenfield's Neuropathology. 1:2400.

Gray DC, Wolfe R, Gee BP, Scoles D, Geng Y, Masella BD, Dubra A, Luque S, Williams DR, Merigan WH (2008) In vivo imaging of the fine structure of rhodamine-labeled macaque retinal ganglion cells. Invest Ophthalmol Vis Sci 49:467-473.

Griffin JW, George EB, Chaudhry V (1996) Wallerian degeneration in peripheral nerve disease. Baillieres Clin Neurol 5:65-75.

Guillemin GJ, Brew BJ (2004) Microglia, macrophages, perivascular macrophages, and pericytes: a review of function and identification. J Leukoc Biol 75:388-397.

Gupta N, Brown KE, Milam AH (2003) Activated microglia in human retinitis pigmentosa, late-onset retinal degeneration, and age-related macular degeneration. Exp Eye Res 76:463-471.

Hall SM (1993) Observations on the progress of Wallerian degeneration in transected peripheral nerves of C57BL/Wld mice in the presence of recruited macrophages. J Neurocytol 22:480-490.

Hartline HK (1938) The response of single optic nerve fibers of the vertebrate eye to illumination of the retina. American Journal of Physiology 121:400-415.

Hecht S, Shlaer S, Pirenne MH (1942) Energy, Quanta, and Vision. J Gen Physiol 25:819-840.

Hickey WF, Kimura H (1988) Perivascular microglial cells of the CNS are bone marrow-derived and present antigen in vivo. Science 239:290-292.

Isayama T, Berson DM, Pu M (2000) Theta ganglion cell type of cat retina. J Comp Neurol 417:32-48.

Ji J, So R, Lor F, Cheung R, Howarth P, Stanney K (2005) A search for possible neural pathways leading to visually induced motion sickness. Vision Res 17:131-134.

Jung S, Aliberti J, Graemmel P, Sunshine MJ, Kreutzberg GW, Sher A, Littman DR (2000) Analysis of fractalkine receptor CX(3)CR1 function by targeted deletion and green fluorescent protein reporter gene insertion. Mol Cell Biol 20:4106-4114.

Kanje M, Lazarewicz J, Ekstrom P, Edstrom A (1985) Ca2+-activated protease activity in frog sciatic nerve: characterization and effect on rapidly transported axonal proteins. Brain Res 327:29-36.

Kerschensteiner M, Schwab ME, Lichtman JW, Misgeld T (2005) In vivo imaging of axonal degeneration and regeneration in the injured spinal cord. Nat Med 11:572-577.

Kezic J, Xu H, Chinnery HR, Murphy CC, McMenamin PG (2008) Retinal microglia and uveal tract dendritic cells and macrophages are not CX3CR1 dependent in their recruitment and distribution in the young mouse eye. Invest Ophthalmol Vis Sci 49:1599-1608.

Kohno T, Inomata H, Taniguchi Y (1982) Identification of microglia cell of the rat retina by light and electron microscopy. Jpn J Ophthalmol 26:53-68.

Kong JH, Fish DR, Rockhill RL, Masland RH (2005) Diversity of ganglion cells in the mouse retina: unsupervised morphological classification and its limits. J Comp Neurol 489:293-310.

Krause TL, Fishman HM, Ballinger ML, Bittner GD (1994) Extent and mechanism of sealing in transected giant axons of squid and earthworms. J Neurosci 14:6638-6651.

Kuwabara T, Cogan DG (1961) Retinal glycogen. Arch Ophthalmol 66:680-688.

Langmann T (2007) Microglia activation in retinal degeneration. J Leukoc Biol 81:1345-1351.

Lee JE, Liang KJ, Fariss RN, Wong WT (2008) Ex vivo dynamic imaging of retinal microglia using time-lapse confocal microscopy. Invest Ophthalmol Vis Sci 49:4169-4176.

Lee YH, Rho YH, Choi SJ, Ji JD, Song GG (2005) Ankylosing spondylitis susceptibility loci defined by genome-search meta-analysis. J Hum Genet 50:453-459.

Leung CK, Lindsey JD, Chen L, Liu Q, Weinreb RN (2009) Longitudinal profile of retinal ganglion cell damage assessed with blue-light confocal scanning laser ophthalmoscopy after ischaemic reperfusion injury. Br J Ophthalmol 93:964-968.

Leung CK, Lindsey JD, Crowston JG, Lijia C, Chiang S, Weinreb RN (2008a) Longitudinal profile of retinal ganglion cell damage after optic nerve crush with blue-light confocal scanning laser ophthalmoscopy. Invest Ophthalmol Vis Sci 49:4898-4902.

Leung CK, Lindsey JD, Crowston JG, Ju WK, Liu Q, Bartsch DU, Weinreb RN (2008b) In vivo imaging of murine retinal ganglion cells. J Neurosci Methods 168:475-478.

Leventhal AG, Rodieck RW, Dreher B (1981) Retinal ganglion cell classes in the Old World monkey: morphology and central projections. Science 213:1139-1142.

Li H, Li SH, Yu ZX, Shelbourne P, Li XJ (2001) Huntingtin aggregate-associated axonal degeneration is an early pathological event in Huntington's disease mice. J Neurosci 21:8473-8481.

Ling EA, Wong WC (1993) The origin and nature of ramified and amoeboid microglia: a historical review and current concepts. Glia 7:9-18.

Lubinska L (1977) Early course of Wallerian degeneration in myelinated fibres of the rat phrenic nerve. Brain Res 130:47-63.

Lucas RJ, Freedman MS, Munoz M, Garcia-Fernandez JM, Foster RG (1999) Regulation of the mammalian pineal by non-rod, non-cone, ocular photoreceptors. Science 284:505-507.

Lunn ER, Perry VH, Brown MC, Rosen H, Gordon S (1989) Absence of Wallerian Degeneration does not Hinder Regeneration in Peripheral Nerve. Eur J Neurosci 1:27-33.

Malpeli JG, Baker FH (1975) The representation of the visual field in the lateral geniculate nucleus of Macaca mulatta. J Comp Neurol 161:569-594.

Marchesi F, Locatelli M, Solinas G, Erreni M, Allavena P, Mantovani A (2010) Role of CX3CR1/CX3CL1 axis in primary and secondary involvement of the nervous system by cancer. J Neuroimmunol 224:39-44.

Martin PR (1986) The projection of different retinal ganglion cell classes to the dorsal lateral geniculate nucleus in the hooded rat. Exp Brain Res 62:77-88.

Mattson MP (1999) Establishment and plasticity of neuronal polarity. J Neurosci Res 57:577-589.

Mattson MP (2000) Apoptotic and anti-apoptotic synaptic signaling mechanisms. Brain Pathol 10:300-312.

Mattson MP, Keller JN, Begley JG (1998a) Evidence for synaptic apoptosis. Exp Neurol 153:35-48.

Mattson MP, Partin J, Begley JG (1998b) Amyloid beta-peptide induces apoptosis-related events in synapses and dendrites. Brain Res 807:167-176.

Meucci O, Fatatis A, Simen AA, Miller RJ (2000) Expression of CX3CR1 chemokine receptors on neurons and their role in neuronal survival. Proc Natl Acad Sci U S A 97:8075-8080.

Morgan JE (2002) Retinal ganglion cell shrinkage in glaucoma. J Glaucoma 11:365-370.

Morris R (1985) Thy-1 in developing nervous tissue. Dev Neurosci 7:133-160.

Muller HW, Minwegen P (1987) Nonresident macrophages in peripheral nerve of rat: effect of silica on migration, myelin phagocytosis, and apolipoprotein E expression during Wallerian degeneration. J Neurosci Res 18:222-229.

Naito J (1989) Retinogeniculate projection fibers in the monkey optic nerve: a demonstration of the fiber pathways by retrograde axonal transport of WGA-HRP. J Comp Neurol 284:174-186.

Nicholls DG (2009) Mitochondrial calcium function and dysfunction in the central nervous system. Biochim Biophys Acta 1787:1416-1424.

Nikolaeva MA, Mukherjee B, Stys PK (2005) Na+-dependent sources of intra-axonal Ca2+ release in rat optic nerve during in vitro chemical ischemia. J Neurosci 25:9960-9967.

Nimmerjahn A, Kirchhoff F, Helmchen F (2005) Resting microglial cells are highly dynamic surveillants of brain parenchyma in vivo. Science 308:1314-1318.

Osborne NN, Casson RJ, Wood JP, Chidlow G, Graham M, Melena J (2004) Retinal ischemia: mechanisms of damage and potential therapeutic strategies. Prog Retin Eye Res 23:91-147.

Ouardouz M, Nikolaeva MA, Coderre E, Zamponi GW, McRory JE, Trapp BD, Yin X, Wang W, Woulfe J, Stys PK (2003) Depolarization-induced Ca2+ release in ischemic spinal cord white matter involves L-type Ca2+ channel activation of ryanodine receptors. Neuron 40:53-63.

Paques M, Simonutti M, Roux MJ, Picaud S, Levavasseur E, Bellman C, Sahel JA (2006) High resolution fundus imaging by confocal scanning laser ophthalmoscopy in the mouse. Vision Res 46:1336-1345.

Paul JA, Gregson NA (1992) An immunohistochemical study of phospholipase A2 in peripheral nerve during Wallerian degeneration. J Neuroimmunol 39:31-47.

Pavlidis M, Stupp T, Naskar R, Cengiz C, Thanos S (2003) Retinal ganglion cells resistant to advanced glaucoma: a postmortem study of human retinas with the carbocyanine dye DiI. Invest Ophthalmol Vis Sci 44:5196-5205.

Perry VH (1979) The ganglion cell layer of the retina of the rat: a Golgi study. Proc R Soc Lond B Biol Sci 204:363-375.

Perry VH, Hume DA, Gordon S (1985) Immunohistochemical localization of macrophages

and microglia in the adult and developing mouse brain. Neuroscience 15:313-326.

Perry VH, Brown MC, Lunn ER, Tree P, Gordon S (1990) Evidence that Very Slow Wallerian Degeneration in C57BL/Ola Mice is an Intrinsic Property of the Peripheral Nerve. Eur J Neurosci 2:802-808.

Pickard GE (1982) The afferent connections of the suprachiasmatic nucleus of the golden hamster with emphasis on the retinohypothalamic projection. J Comp Neurol 211:65-83.

Provis JM, Diaz CM, Penfold PL (1996) Microglia in human retina: a heterogeneous population with distinct ontogenies. Perspect Dev Neurobiol 3:213-222.

Quigley HA, Dunkelberger GR, Green WR (1988) Chronic human glaucoma causing selectively greater loss of large optic nerve fibers. Ophthalmology 95:357-363.

Quigley HA, Sanchez RM, Dunkelberger GR, L'Hernault NL, Baginski TA (1987) Chronic glaucoma selectively damages large optic nerve fibers. Invest Ophthalmol Vis Sci 28:913-920.

Reichert F, Levitzky R, Rotshenker S (1996) Interleukin 6 in intact and injured mouse peripheral nerves. Eur J Neurosci 8:530-535.

Remtulla S, Hallett PE (1985) A schematic eye for the mouse, and comparisons with the rat. Vision Res 25:21-31.

Rhodin JA, Fujita H (1989) Capillary growth in the mesentery of normal young rats. Intravital video and electron microscope analyses. J Submicrosc Cytol Pathol 21:1-34.

Ristanovic D, Milosevic NT, Stulic V (2006) Application of modified Sholl analysis to

neuronal dendritic arborization of the cat spinal cord. J Neurosci Methods 158:212-218.

Rockhill RL, Daly FJ, MacNeil MA, Brown SP, Masland RH (2002) The diversity of ganglion cells in a mammalian retina. J Neurosci 22:3831-3843.

Rodieck RW, Watanabe M (1993) Survey of the morphology of macaque retinal ganglion cells that project to the pretectum, superior colliculus, and parvicellular laminae of the lateral geniculate nucleus. J Comp Neurol 338:289-303.

Rodieck RW, Binmoeller KF, Dineen J (1985) Parasol and midget ganglion cells of the human retina. J Comp Neurol 233:115-132.

Sabel BA, Engelmann R, Humphrey MF (1997) In vivo confocal neuroimaging (ICON) of CNS neurons. Nat Med 3:244-247.

Schlaepfer WW (1971) Experimental alterations of neurofilaments and neurotubules by calcium and other ions. Exp Cell Res 67:73-80.

Schlaepfer WW (1974) Calcium-induced degeneration of axoplasm in isolated segments of rat peripheral nerve. Brain Res 69:203-215.

Schroeter M, Jander S (2005) T-cell cytokines in injury-induced neural damage and repair. Neuromolecular Med 7:183-195.

Shou TD, Zhou YF (1989) Y cells in the cat retina are more tolerant than X cells to brief elevation of IOP. Invest Ophthalmol Vis Sci 30:2093-2098.

Smith GG BC (1952) Survival time of retinal cells when deprived of their blood supply by increased intraocular pressure. Am J Ophthalmol 35:133-136.

Sparrow JR, Zhou J, Ben-Shabat S, Vollmer H, Itagaki Y, Nakanishi K (2002) Involvement of oxidative mechanisms in blue-light-induced damage to A2E-laden RPE. Invest Ophthalmol Vis Sci 43:1222-1227.

Spencer PS, Schaumburg HH (1977a) Ultrastructural studies of the dying-back process. III. The evolution of experimental peripheral giant axonal degeneration. J Neuropathol Exp Neurol 36:276-299.

Spencer PS, Schaumburg HH (1977b) Ultrastructural studies of the dying-back process. IV. Differential vulnerability of PNS and CNS fibers in experimental central-peripheral distal axonopathies. J Neuropathol Exp Neurol 36:300-320.

Stokin GB, Lillo C, Falzone TL, Brusch RG, Rockenstein E, Mount SL, Raman R, Davies P, Masliah E, Williams DS, Goldstein LS (2005) Axonopathy and transport deficits early in the pathogenesis of Alzheimer's disease. Science 307:1282-1288.

Stoll G, Jung S, Jander S, van der Meide P, Hartung HP (1993) Tumor necrosis factor-alpha in immune-mediated demyelination and Wallerian degeneration of the rat peripheral nervous system. J Neuroimmunol 45:175-182.

Stone J, Clarke R (1980) Correlation between soma size and dendritic morphology in cat retinal ganglion cells: evidence of further variation in the gamma-cell class. J Comp Neurol 192:211-217.

Stys PK (2004) White matter injury mechanisms. Curr Mol Med 4:113-130.

Sun W, Li N, He S (2002a) Large-scale morphological survey of mouse retinal ganglion cells. J Comp Neurol 451:115-126.

Sun W, Li N, He S (2002b) Large-scale morophological survey of rat retinal ganglion cells. Vis Neurosci 19:483-493.

Suzumura A, Mezitis SG, Gonatas NK, Silberberg DH (1987) MHC antigen expression on bulk isolated macrophage-microglia from newborn mouse brain: induction of Ia antigen expression by gamma-interferon. J Neuroimmunol 15:263-278.

Szmajda BA, Grunert U, Martin PR (2008) Retinal ganglion cell inputs to the koniocellular pathway. J Comp Neurol 510:251-268.

Thanos S (1992) Sick photoreceptors attract activated microglia from the ganglion cell layer: a model to study the inflammatory cascades in rats with inherited retinal dystrophy. Brain Res 588:21-28.

Thanos S, Indorf L, Naskar R (2002) In vivo FM: using conventional fluorescence microscopy to monitor retinal neuronal death in vivo. Trends Neurosci 25:441-444.

Thomas WE (1999) Brain macrophages: on the role of pericytes and perivascular cells. Brain Res Brain Res Rev 31:42-57.

Thompson H, Barker D, Camand O, Erskine L (2006) Slits contribute to the guidance of retinal ganglion cell axons in the mammalian optic tract. Dev Biol 296:476-484.

Uutela M, Wirzenius M, Paavonen K, Rajantie I, He Y, Karpanen T, Lohela M, Wiig H, Salven P, Pajusola K, Eriksson U, Alitalo K (2004) PDGF-D induces macrophage recruitment, increased interstitial pressure, and blood vessel maturation during angiogenesis. Blood 104:3198-3204.

Van Der Velden HA (1946) The number of quanta necessary for the perception of light of the human eye. Ophthalmologica 111:321-331.

Venezie RD, Toews AD, Morell P (1995) Macrophage recruitment in different models of nerve injury: lysozyme as a marker for active phagocytosis. J Neurosci Res 40:99-107.

Vrabec F (1970) Microglia in the monkey and rabbit retina. J Neuropathol Exp Neurol 29:217-224.

Walsh MK, Quigley HA (2008) In vivo time-lapse fluorescence imaging of individual retinal ganglion cells in mice. J Neurosci Methods 169:214-221.

Walton PD, Airey JA, Sutko JL, Beck CF, Mignery GA, Sudhof TC, Deerinck TJ, Ellisman MH (1991) Ryanodine and inositol trisphosphate receptors coexist in avian cerebellar Purkinje neurons. J Cell Biol 113:1145-1157.

Wang L, Dong J, Cull G, Fortune B, Cioffi GA (2003) Varicosities of intraretinal ganglion cell axons in human and nonhuman primates. Invest Ophthalmol Vis Sci 44:2-9.

Watanabe M, Rodieck RW (1989) Parasol and midget ganglion cells of the primate retina. J Comp Neurol 289:434-454.

Watanabe M, Fukuda Y (2002) Survival and axonal regeneration of retinal ganglion cells in adult cats. Prog Retin Eye Res 21:529-553.

Webb RH, Hughes GW, Delori FC (1987) Confocal scanning laser ophthalmoscope. Appl Opt 26:1492-1499.

Weber AJ, Kaufman PL, Hubbard WC (1998) Morphology of single ganglion cells in the glaucomatous primate retina. Invest Ophthalmol Vis Sci 39:2304-2320.

Whitmore AV, Libby RT, John SW (2005) Glaucoma: thinking in new ways-a role for autonomous axonal self-destruction and other compartmentalised processes? Prog Retin Eye Res 24:639-662.

Wong KY, Dunn FA, Berson DM (2005) Photoreceptor adaptation in intrinsically photosensitive retinal ganglion cells. Neuron 48:1001-1010.

Yin Y, Cui Q, Li Y, Irwin N, Fischer D, Harvey AR, Benowitz LI (2003) Macrophage-derived factors stimulate optic nerve regeneration. J Neurosci 23:2284-2293.

Zalewska T, Kanje M, Edstrom A (1986) A calcium-activated neutral protease in the frog nervous system which degrades rapidly transported axonal proteins. Brain Res 381:58-62.

Zhu Y, Ohlemiller KK, McMahan BK, Gidday JM (2002) Mouse models of retinal ischemic tolerance. Invest Ophthalmol Vis Sci 43:1903-1911.

Figures

Name of cell	**Location**
Epithelioid cells	Granulomas
Sinusoidal lining cells	Spleen
Kupffer cells	Liver
Microglia	Neural tissue
Dust cells/Alveolar macrophages	Pulmonary alveolus of lungs
Osteoclasts	Bone
Histiocytes	Connective tissue
Mesangial cells	Kidney

Table 1.1 The specific name of macrophages according their locations.

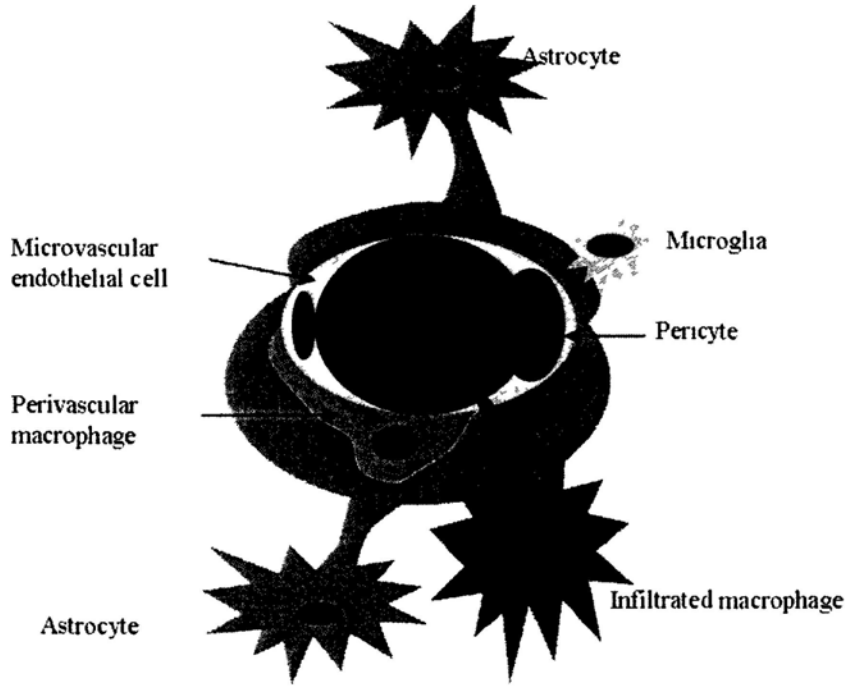

Figure 1.1 A schematic diagram for the location of different subsets of macrophages in central nerve system (CNS).

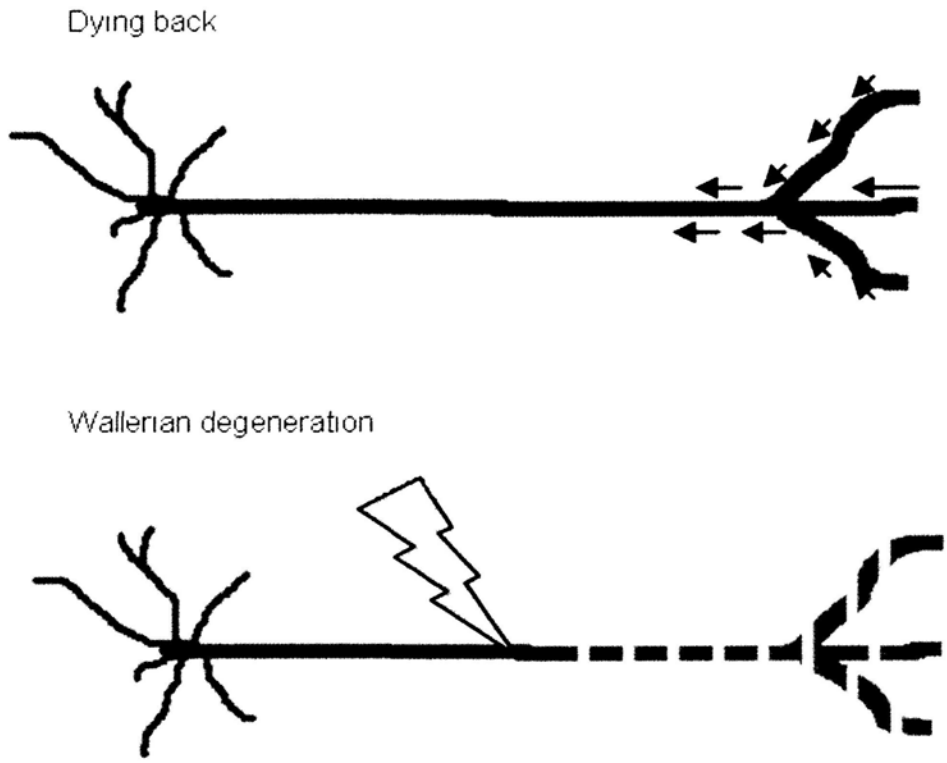

Figure 1.2 A schematic diagram illustrating dying back and wallerian degeneration. Wallerian degeneration can be induced by focal severe injury, followed by destruction of distal axon. In dying back, the axon degenerates at the distal end towards the cell body.

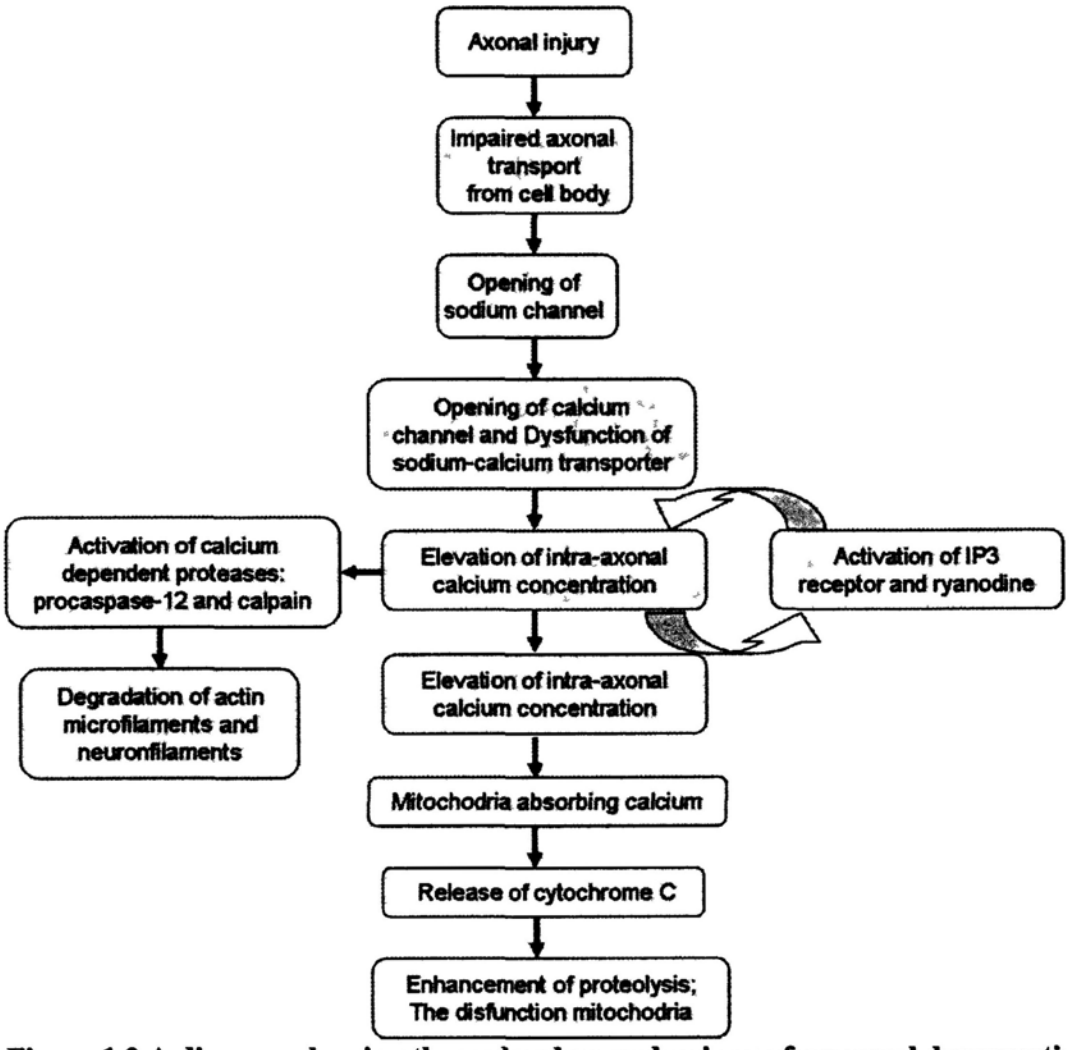

Figure 1.3 A diagram showing the molecular mechanisms of neuronal degeneration.

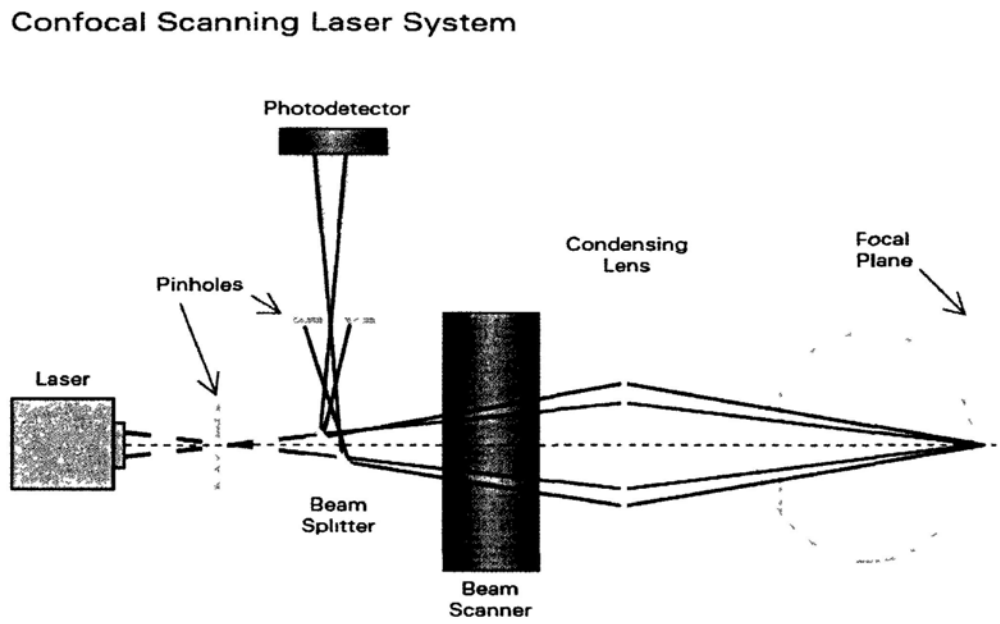

Figure 1.4 A schematic diagram of a confocal laser scanning ophthalmoscope.

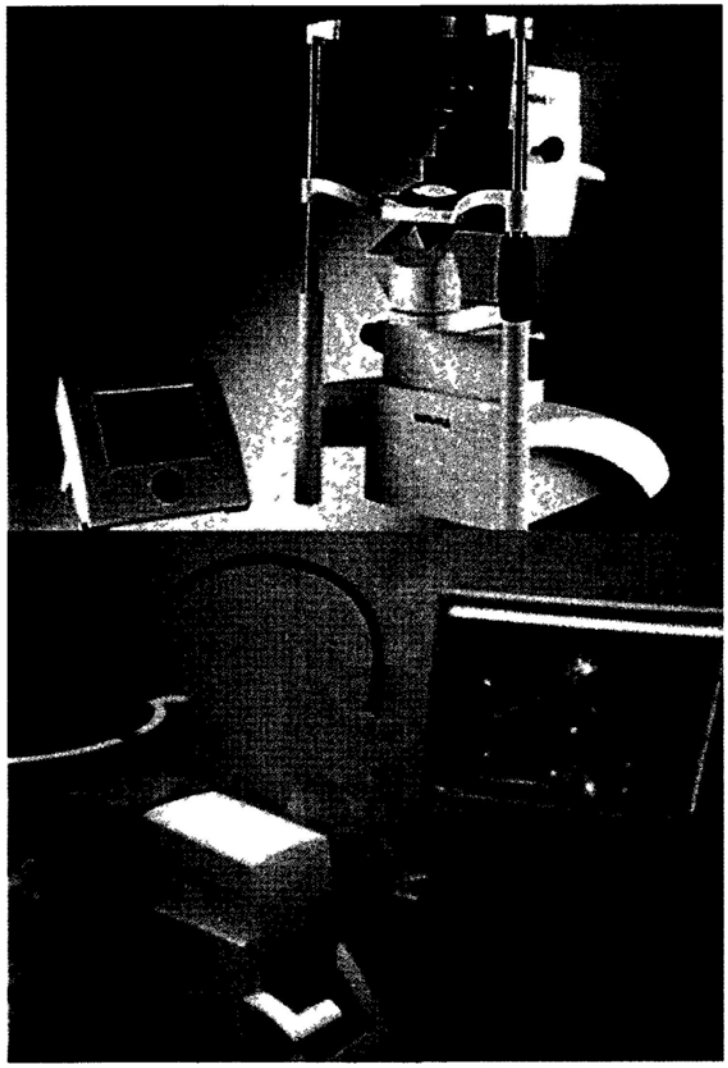

Figure 3.1 *In vivo* imaging on a THY1-YFP transgenic mouse with CSLO. An CSLO unit (HRA2, Heidelberg Engineering, GmbH, Dossenheim, Germany) was used for RGCs imaging. A 55 degree wide field lens was added to the camera to increase the field of view of the fundus. Fifteen images at the same retinal location were captured, averaged automatically by the built-in software to augment the signal-to-noise ratio and simultaneously displayed on a computer screen.

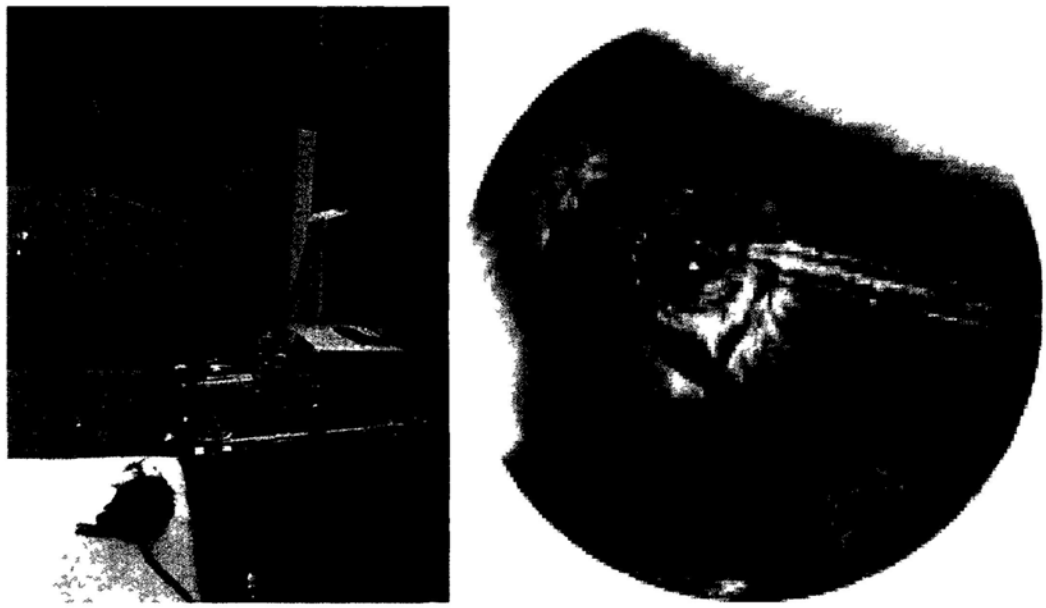

Figure 3.2 Retinal ischemia induced by acute elevation of intraocular pressure (IOP).

A micro-injection glass pipette was fixed at the manipulating arm of the SR-6N stereotaxic instrument (Narishige Scientific Instrument Laboratory, Tokyo, Japan). The pipette was connected to a container with 500 ml sterile normal saline. The container was raised to elevate the IOP to 110 mmHg.

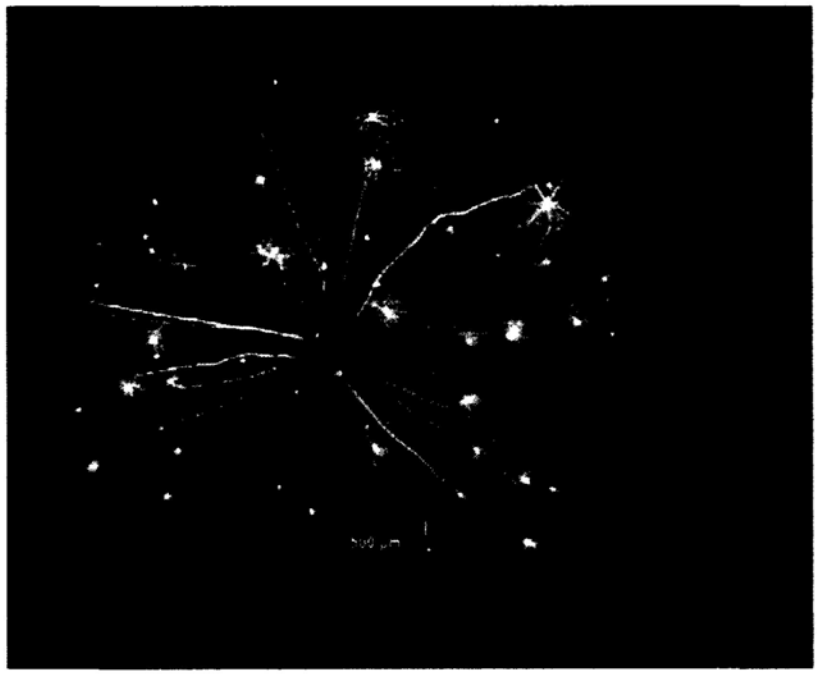

Figure 4.1a A retinal montage constructed from 12 image captures obtained from *in vivo* imaging on THY1-YFP transgenic mice with CSLO.

Figure 4.1b A retinal ganglion cell imaged by the CLSO *in vivo* (left) and a confocal microscope on retinal flatmount (right). The number and the branching of dendritic arborization imaged by the CSLO have direct correspondence with those observed in the retinal wholemount.

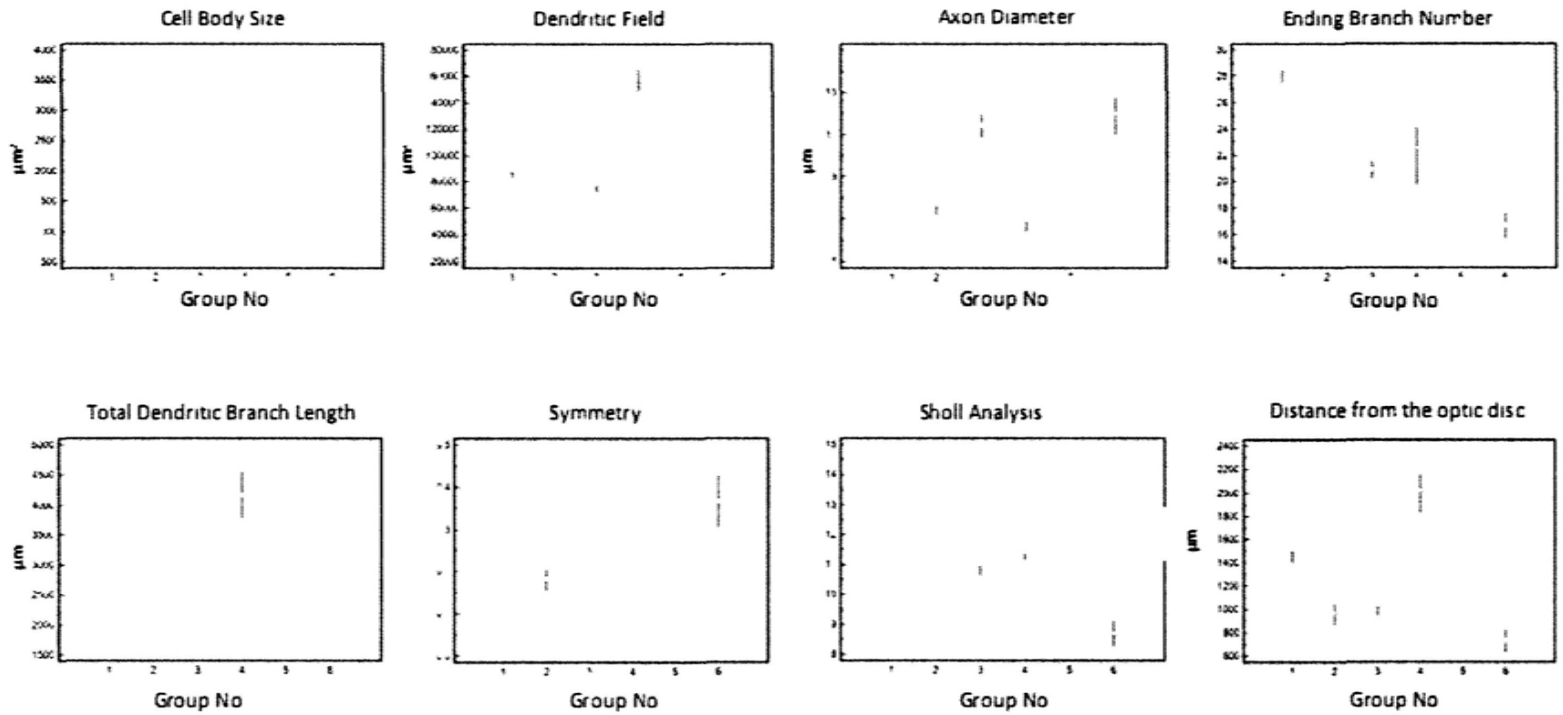

Figure 4.2 Classification of a total of 125 RGCs from 16 retinas with clear axonal and dendritic structures visualized by the CSLO.

Cluster analysis identified 6 groups of RGCs with reference to 8 morphological and anatomical parameters (cell body size, axonal diameter, dendritic field size, ending branch number, total dendritic branch length, symmetry, branching complexity (Sholl analysis), and distance from the optic disc) .

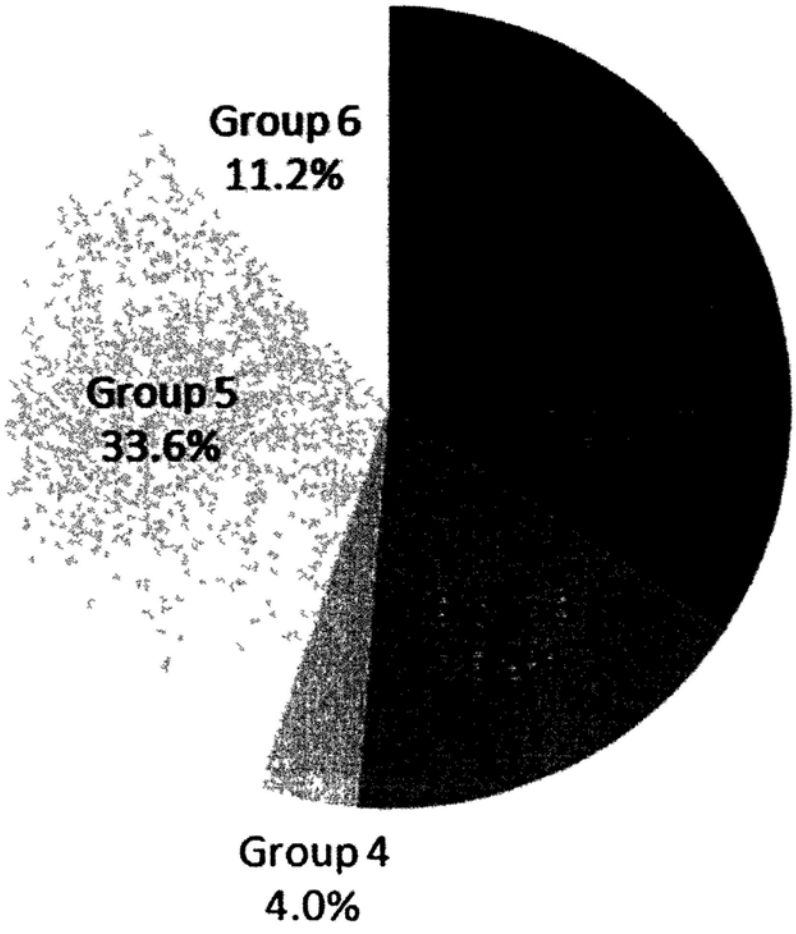

Figure 4.3 Proportion of different subgroups of retinal ganglion cells classified by cluster analysis.

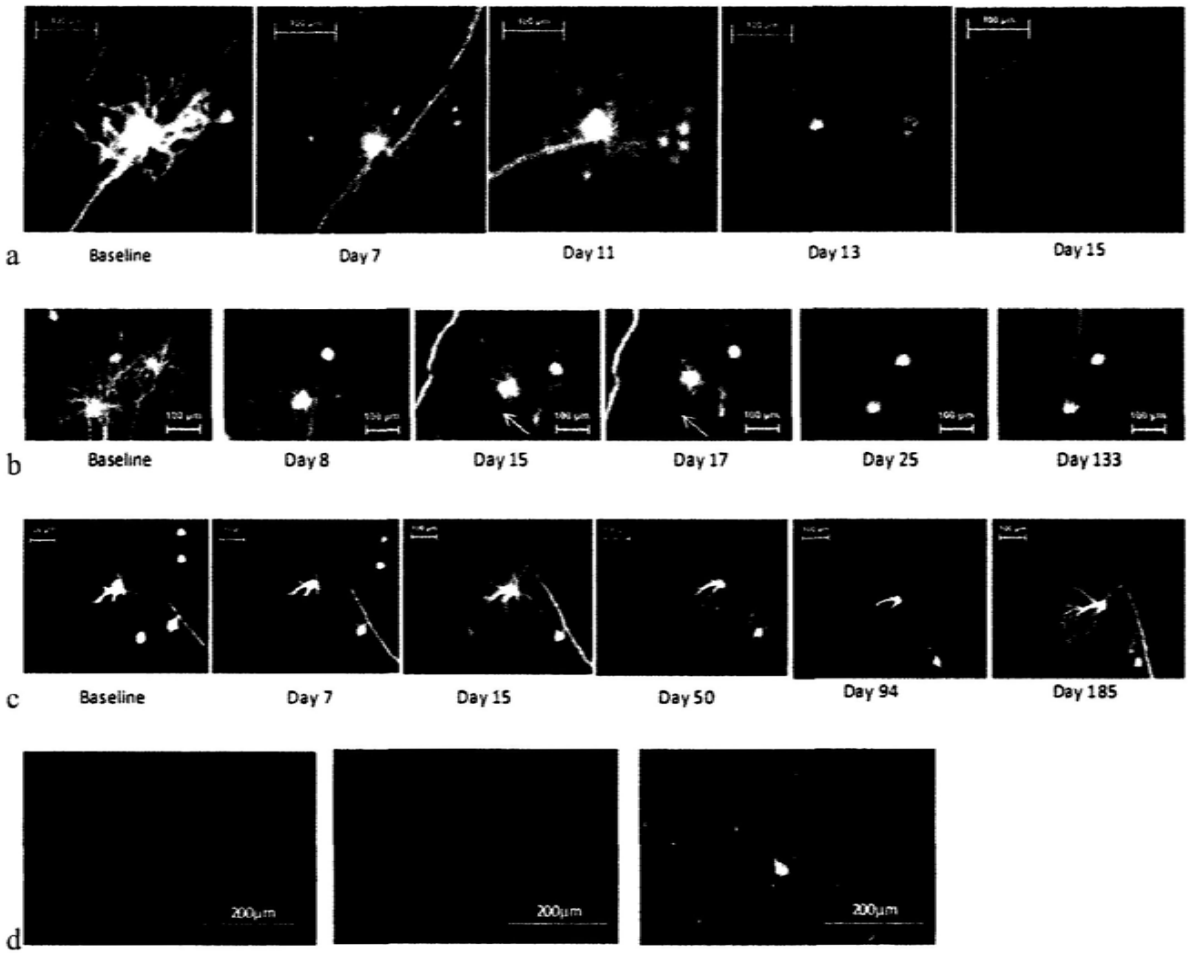
a
Baseline
Day 7
Day 11
Day 13
Day 15
b
Baseline
Day 8
Day 15
Day 17
Day 25
Day 133
c
Baseline
Day 7
Day 15
Day 50
Day 94
Day 185
d
200µm
200µm
200µm

Figure 4.4 The longitudinal profiles of RGC degeneration after optic nerve crush. Most RGCs demonstrated progressive dendritic shrinkage followed by loss of the axons and the cell bodies (n=84, 68.3%) (a). Some RGCs had cell bodies detectable for more than 1 to 3 months in the absence of dendritic and axonal structures (n=9, 7.3%) (b). A significant proportion of RGCs (n=26, 21.1%) showed only partial loss of dendritic structures without loss of the axons and the cell bodies at 6 months after the injury (c). Immunohistochemical staining with anti-SMI-32 indicated that the dendritic shrinkage was not due to redistribution of cytoplasmic YFP (d)

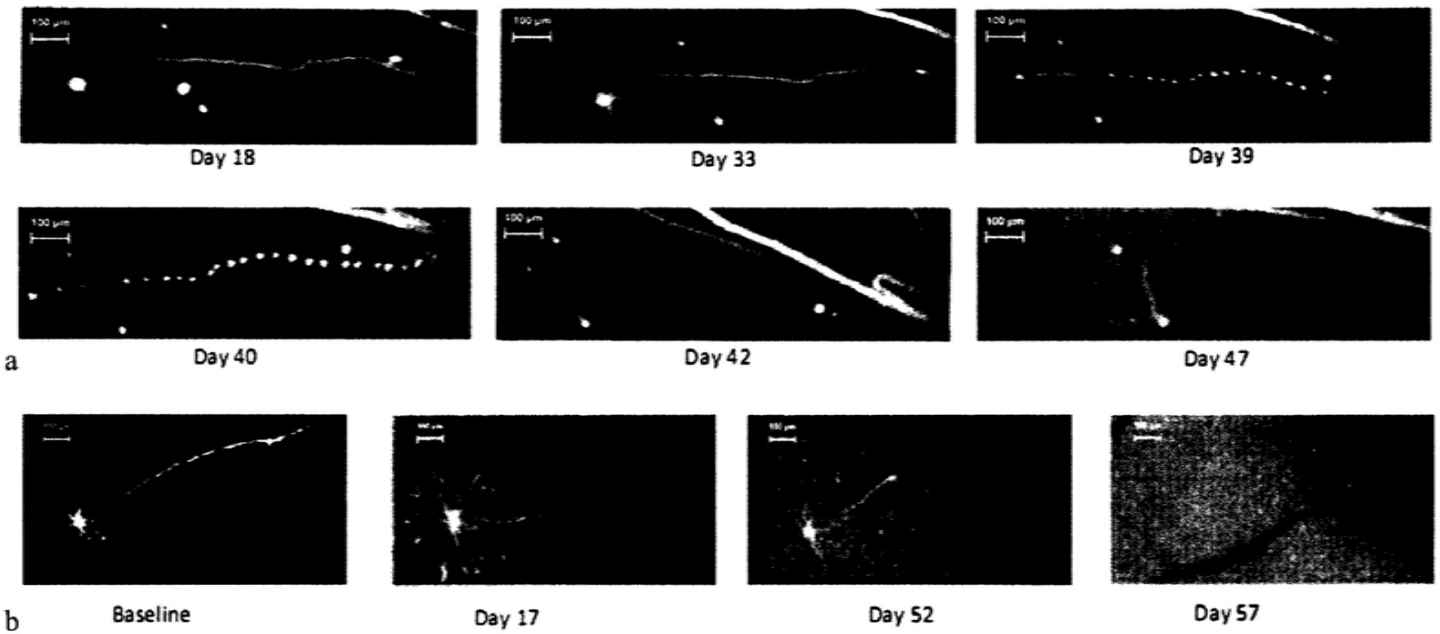

Figure 4.5 The demonstration of wallerian degeneration and axon retraction after optice nerve crush. Progressive axonal changes were only observed in a few RGCs. In 3 RGCs (2.4%), Wallerian degeneration with fragmentation and beading of the axon was observed following progressive dendritic shrinkage (a). In one RGC (0.8%), the proximal axon showedretraction and bulb formation before cell death (Figure b).

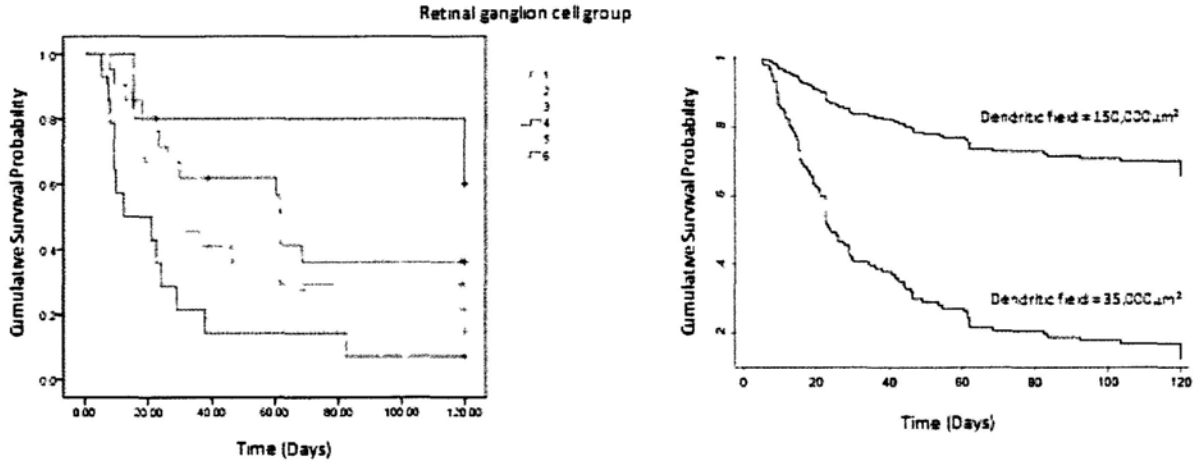

a b

Figure 4.6 Survival analysis for morphological predictive factor for RGC survival after optic nerve injury.

Survival analysis showed that group 4 RGCs had the best survival function and group 6 had the worst. Figure 4.6b compared the predicted survival probability of RGCs with a large (150,000 μm^2) and a small (35,000 μm^2) dendritic field after standardizing other morphological measurements. At one month after optic nerve crush, the survival probabilities were 0.85 and 0.45, respectively.

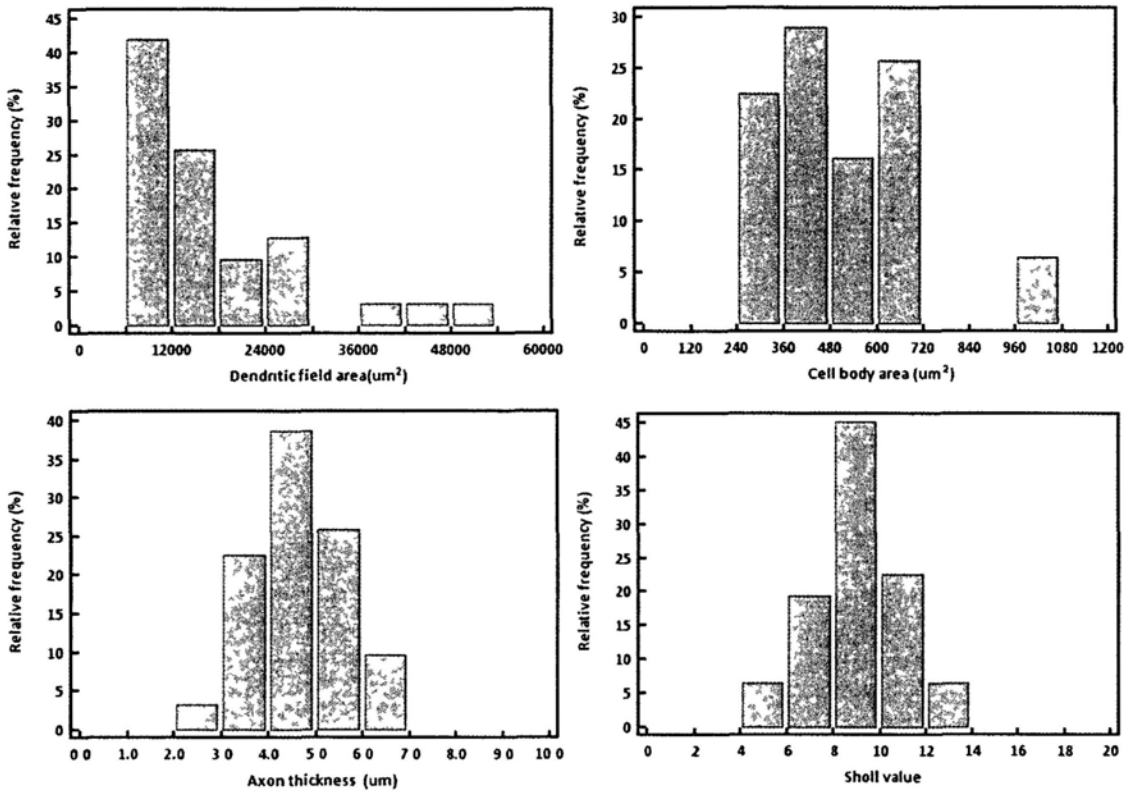

Figure 4.7 Baseline morphological measurements of the 31 retinal ganglion cells. The mean dendritic field, dendritic branching complexity, axonal diameter and cell body area were 17770.3μm², 9.0 (modified Sholl analysis (Ristanovic et al., 2006)), 4.6μm and 499.0μm², and the ranges were 6547.2μm² – 49944.2μm², 5.448 – 12.325, 2.8μm – 6.6μm, and 260.9μm² –1036.2μm², respectively.

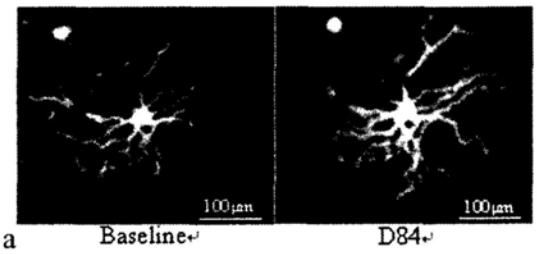

a Baseline D84

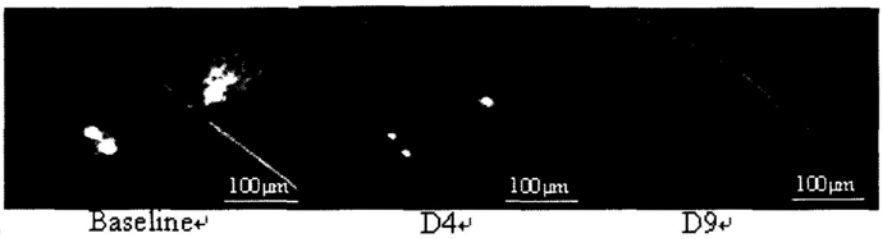

b Baseline D4 D9

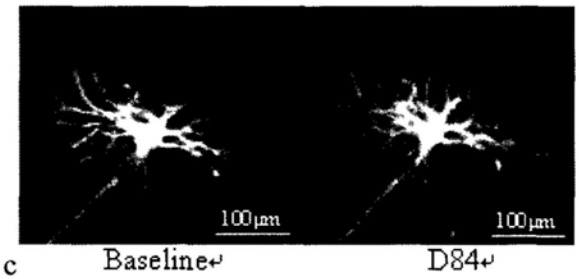

c Baseline D84

Figure 4.8 Longitudinal profiles of retinal ganglion cell degeneration after ischemic injury. There were no detectable changes in axonal or dendritic structures after 30 minutes(n=12) (a) of ischemia. After 90 minutes of ischemia, 78.9% (n=15) of RGCs showed progressive loss of the dendrites, the axon and then the cell body at 1-2 weeks after the injury (b). Complete loss of dendritic tree was evident as early as day 3 after the injury. 21.1% (n=4) had no detectable changes at 3 months after the injury (c).

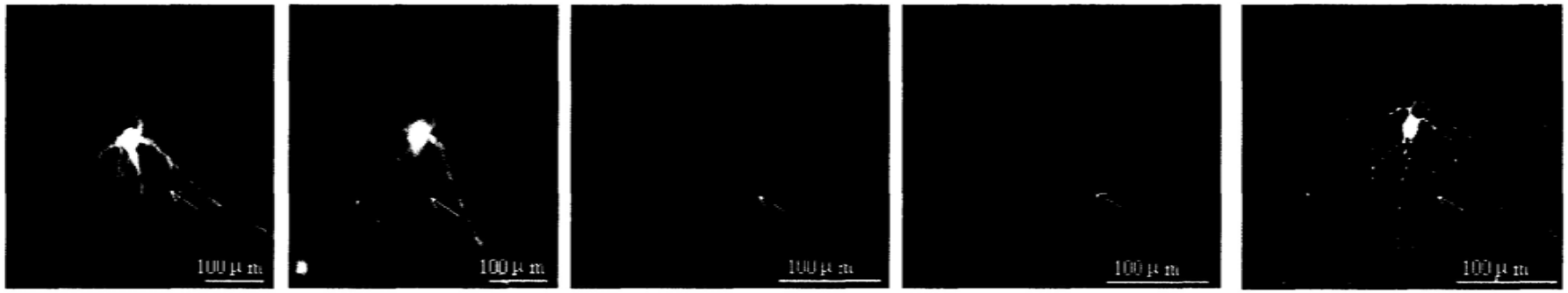

a b c d e

Figure 4.9 A retinal ganglion cell showing loss of dendrites (arrow) and shrinkage of dendritic tree 3 months after 90 minutes of retinal ischemia visualized *in vivo* with a confocal scanning laser ophthalmoscope (a) and (b), and in a retinal flat mount under a confocal scanning laser microscope (c) – (e). At baseline, the dendritic field and dendritic branching complexity (modified Sholl analysis) were 45483.4μm^2 and 11.7, respectively (a). Three months after retinal ischemia, they were 41556.1μm^2 and 11.3, respectively (b). The retina was dissected immediately after the last *in vivo* image capture and stained with anti-SMI32, an anti-neurofilament antibody. The co-localization (e) between YFP (c) and anti-SMI32 (d) suggests that the dendritic changes observed *in vivo* were not secondary to a redistribution of cytoplasmic YFP.

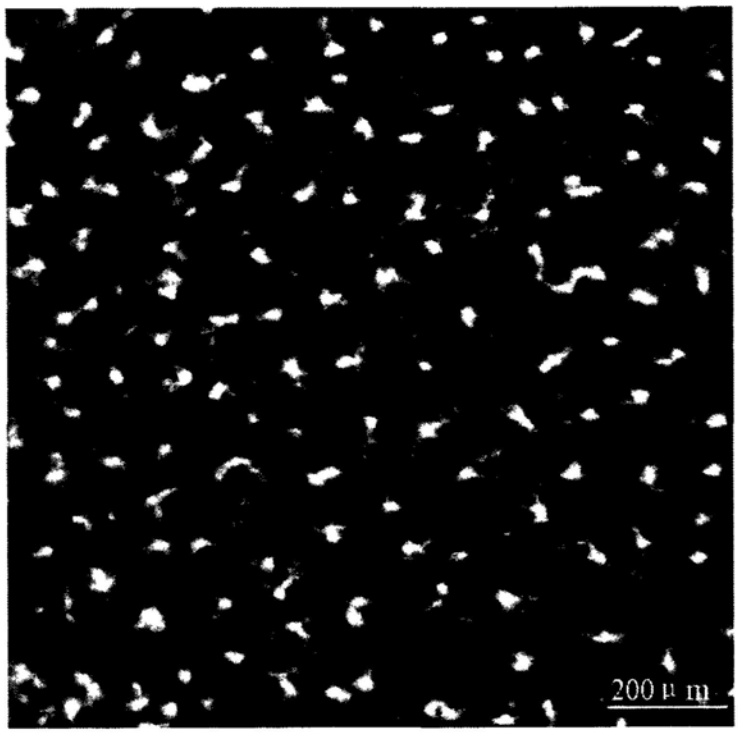

Figure 4.10 *In vivo* imaging of retinal microglia in the CX3CR1$^{GFP/+}$ transgenic mice obtained with an CSLO. The cell bodies and dendrites of resting microglia can be vividly visualized.

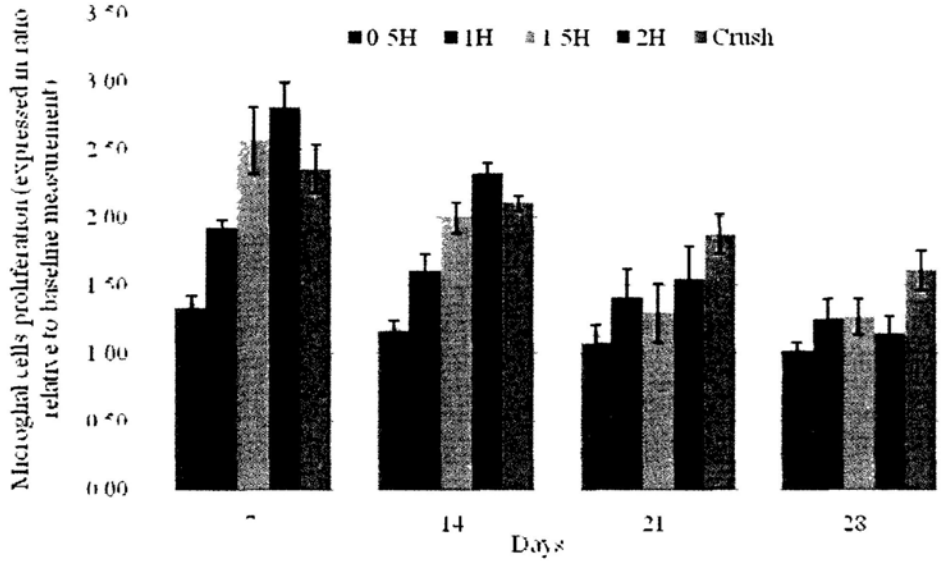

Figure 4.11 The longitudinal profile of retinal microglia activation after optic nerve crush and retinal ischemia. After optic nerve crush (n=4), there was more than two-fold proliferation of retinal microglia evident at week 1. The number of microglia gradually decline with 2.1+/-0.1, 1.9+/-0.2 and 1.6+/-0.1 fold increase at week 2, 3 and 4, respectively. The longitudinal profile of microglia proliferation followed a similar pattern after retinal ischemia induced by elevating the intraocular pressure at 110mmHg with a peak observed at week 1 followed by a gradual decline in the following weeks. The increase in cell density was proportional to the duration of ischemia. At week 1, there were 1.3+/-0.1, 1.9+/-0.1, 2.3+/-0.3 and 2.8+/-0.2 fold increase in microglia after 30, 60, 90 and 120 minutes of ischemia, respectively.

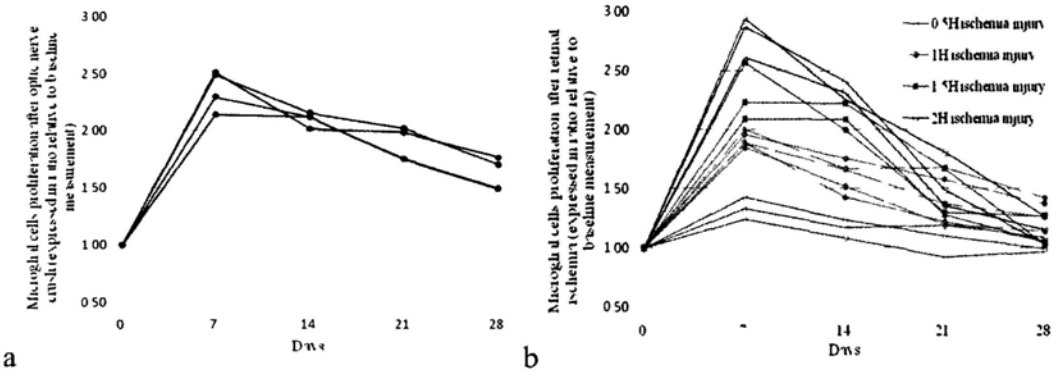

Figure 4.12 Activated microglia time curves showing the longitudinal profiles of microglia proliferation of 18 eyes after optic nerve crush (a) or retinal ischemic injury (b).

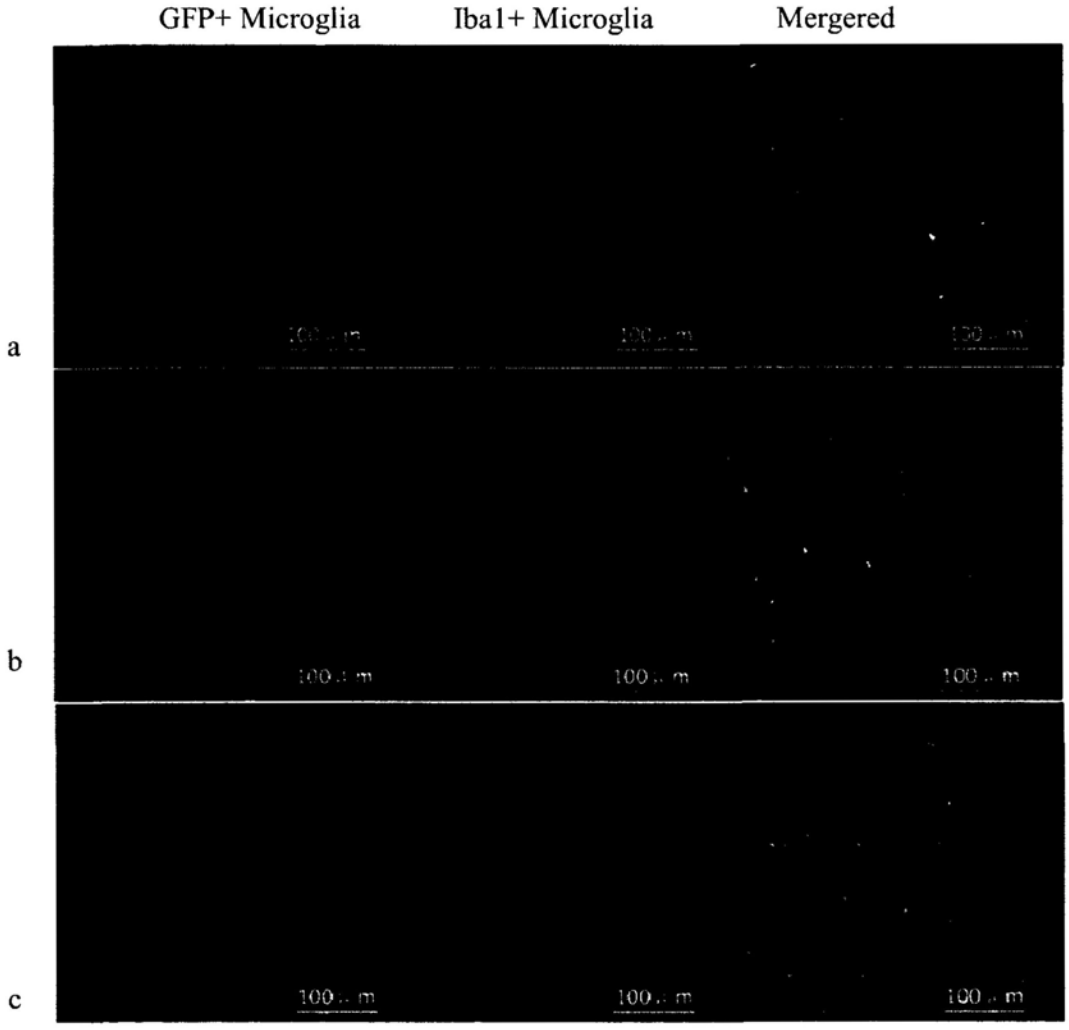

Figure 4.13 Confocal microscopy images showing the correspondence between GFP and Iba1 after 30 minutes (a), 90 minutes (b) of retinal ischemia and optic nerve crush (c). Retinas were dissected at 7 days after the injury.

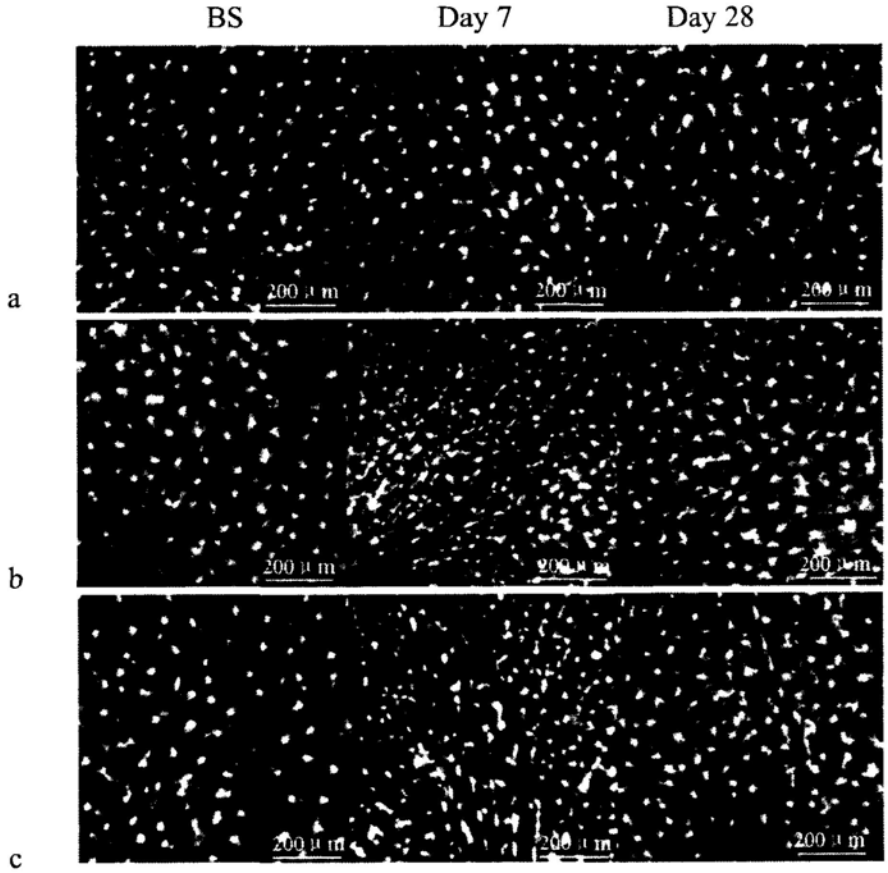

Figure 4.14 *In vivo* images of microglia captured at baseline, day 7 and day 28 after, 30 minutes (a), 90 minutes (b) of retinal ischemia, and optic nerve crush (c).

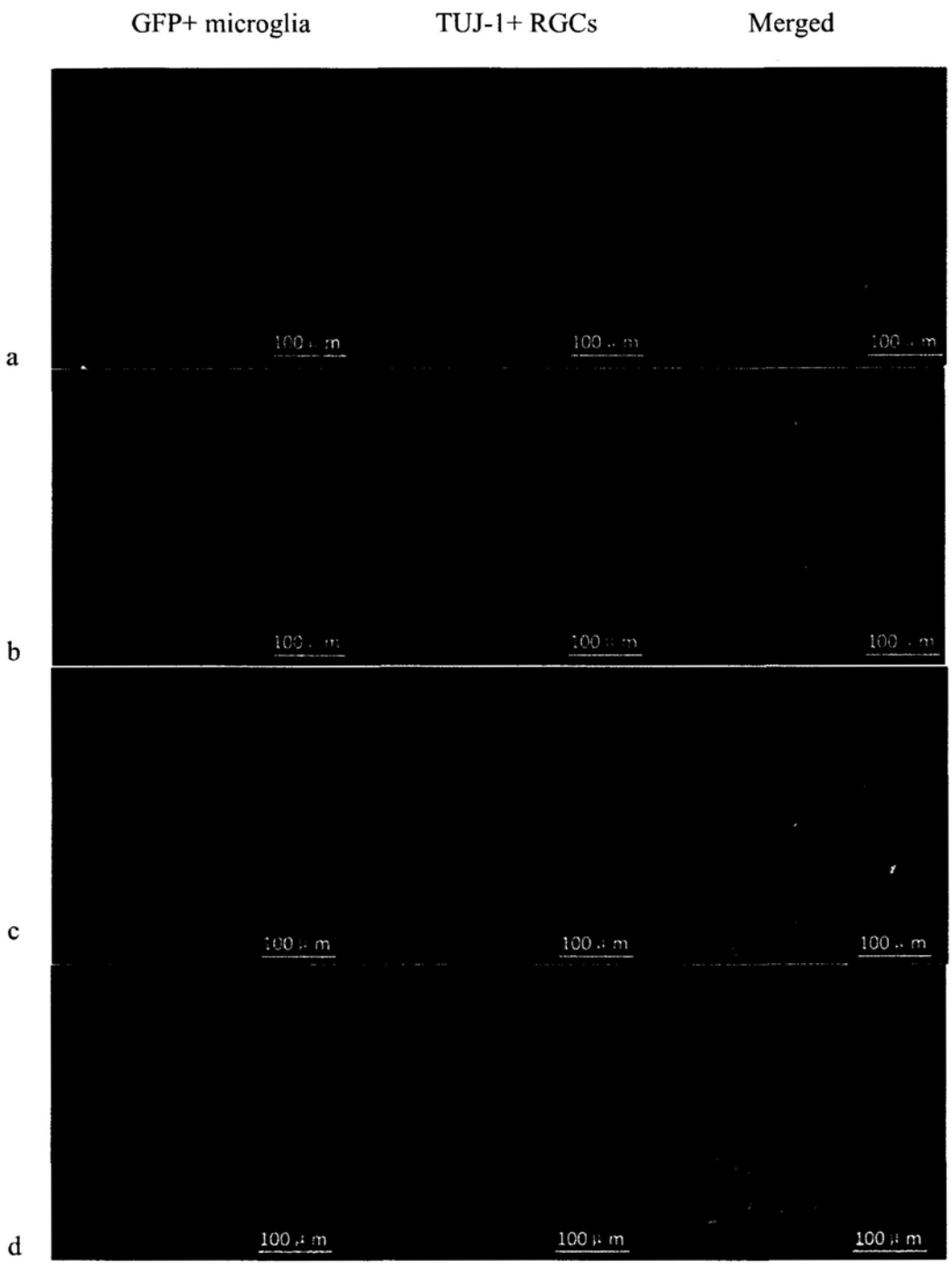

Figure 4.15 Confocal microscopy images showing TUJ1 positive RGCs and GFP positive microglia at the resting state (a), after 30 minutes (b) 90 minutes of retinal ischemia (c), and after optic nerve crush (d). Retinas were dissected at 28 days after the injury.

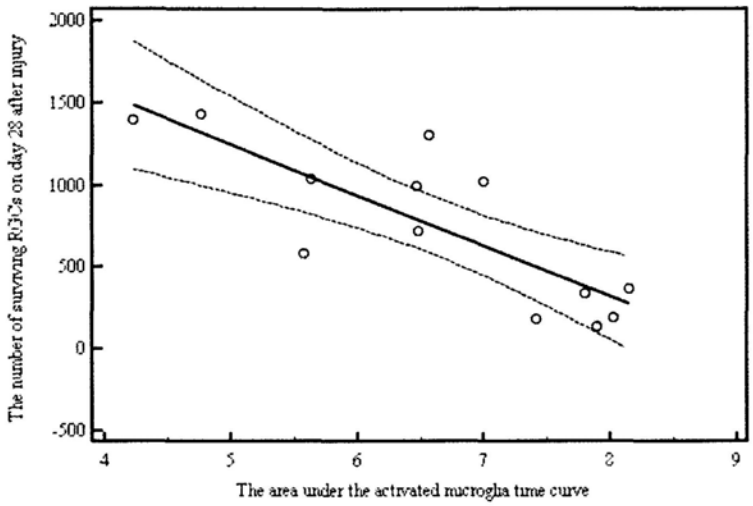

Figure 4.16 Association between of microglia activation and retinal ganglion cells survival. There was a significant association between the number of RGC surviving at week 4 and the area under activated microglia time curve ($P<0.001$). (n=13)